行政院國家科學委員會專題研究計畫 成果報告

迷你乳化聚合製備次微米高分子功能性複合乳膠顆粒(3/3)
研究成果報告(完整版)

計 畫 類 別 ：個別型
計 畫 編 號 ：NSC 95-2221-E-002-152-
執 行 期 間 ：95 年 08 月 01 日至 96 年 07 月 31 日
執 行 單 位 ：國立臺灣大學化學工程學系暨研究所

計 畫 主 持 人：邱文英

計畫參與人員：博士班研究生-兼任助理：羅盈達、郭國輝、陳嘉甫
碩士班研究生-兼任助理：彭郁翔、周琦恩

報 告 附 件 ：出席國際會議研究心得報告及發表論文

處 理 方 式 ：本計畫可公開查詢

中 華 民 國 96 年 10 月 22 日

行政院國家科學委員會補助專題研究計畫 ■ 成 果 報 告
□期中進度報告

迷你乳化聚合製備次微米高分子功能性複合乳膠顆粒(3/3)

計畫類別：■ 個別型計畫　□ 整合型計畫
計畫編號：NSC －95－ 2221－ E－ 002－ 152
執行期間： 95 年 8 月 1 日至 96 年 7 月 31 日

計畫主持人：邱文英
共同主持人：
計畫參與人員： 羅盈達,郭國輝,陳嘉甫,彭郁翔,周琦恩

成果報告類型(依經費核定清單規定繳交)：□精簡報告 ■完整報告

本成果報告包括以下應繳交之附件：
□赴國外出差或研習心得報告一份
□赴大陸地區出差或研習心得報告一份
■出席國際學術會議心得報告及發表之論文各一份
□國際合作研究計畫國外研究報告書一份

處理方式：除產學合作研究計畫、提升產業技術及人才培育研究計畫、列管計畫及下列情形者外，得立即公開查詢
□涉及專利或其他智慧財產權，□一年□二年後可公開查詢

執行單位：國立臺灣大學化學工程學系暨研究所

中 華 民 國 96 年 10 月 22 日

迷你乳化聚合製備次微米高分子功能性複合乳膠顆粒(3/3)

計劃編號：NSC-95-2221-E-002-152

執行期限：95 年8 月1 日至96 年7 月31 日

計劃主持人：邱文英 (Wen-Yen Chiu) 國立台灣大學化工所

PART Ⅰ：Preparation of latex particles: one to one copy of monomer droplets via a modified miniemulsion polymerization

ABSTRACT:

One to one copy the monomer droplets to latex particles was fulfilled entirely via a modified miniemulsion polymerization in this work when the initiator, 2,2'-Azobisisobutyronitrile, was used. The character of the modified process was that polymerization was not carried out after homogenization immediately and enough equilibrium time was provided for the miniemulsion to reach a more stable state. The advantage of the modified process was that, the size distribution was narrow and the particle size was adjustable from tens of nanometers to hundreds of nanometers. The larger latex particles could be obtained with 100% droplet nucleation mechanism for this modified process rather than the smaller ones produced in our earlier work from a conventional miniemulsion polymerization. Moreover, it was possible to preserve the one-to-one feature of latex particles even though the costabilizer was absent. The importance of costabilizer for miniemulsion polymerization was related to the surfactant concentration. When initiator was changed from oil soluble to water soluble, the feature of one-to-one disappeared, that was because the fluctuation was large and the stability of droplets was destroyed when free radicals were generated in aqueous phase.

Keywords: Droplet nucleation; Narrow size distribution; Miniemulsion polymerization

INTRODUCTION

In conventional emulsion polymerization, droplets with size larger than μm served as a monomer reservoir and latex particles nucleated either in monomer swollen micelles or aqueous phase[1, 2]. However, in miniemulsion polymerization, the size of droplets was reduced substantially to 50nm-500nm[3] by variety of homogenized process such as ultrasonication[4-6], high-pressure homogenizer[7, 8]and other high shear devices[9]. The droplets with more O/W surface area could compete with micelles to capture free radicals. As a result, monomer droplets could act as a nanoreactors and polymerized in situ, that was called droplet nucleation[10, 11]. Because of the characteristic of miniemulsion polymerization, the size distributions of monomer droplets should be identical to latex particles ideally. Unfortunately, homogeneous/micellar nucleation could not be rule out in most cases in fact. One reason was the stability of miniemulsion was insufficient to resist coalescence and Ostwald ripening. Coalescence could be avoided by adequate amount of ionic or nonionic surfactant to stabilize the O/W surface from droplet collision. The cause of Ostwald ripening was due to that the solubility of monomer in water was increasing with decreasing monomer droplets size and the size of larger monomer droplets grew by expensing smaller monomer droplets.[12-14] In order to retard destabilization from monomer diffusion, hydrophobic costabilizer like fatty alcohols[15] or long-chain alkanes[16, 17] were used as trapped species in miniemulsion to build up a counteracting osmotic pressure. Webster and Cates[18] established the stabilization effect of emulsion with trapped species in droplets theoretically. Three regions with different stability of droplets was found, R_B and R_S was the boundary between these three regions, R present the radius of droplet and subscripts B and S denoted as balance and stability. When the size of droplet was larger than R_B (region Ⅲ), the emulsion was unstable and droplet would coarsen immediately. If the size of droplets was smaller than R_S (region Ⅰ), the emulsion was fully stable. In region Ⅱ, the size of droplet lied between R_B and R_S, the emulsion was metastable, coarsening occurred when there was a fluctuation in local environment of droplet or a few larger droplets existed in the initial state.

In our previous study and other researches, polymerization was carried out immediately after miniemulsion was homogenized, and the kinetics or nucleation mechanism was investigated[19-22]. In this way, homogenized energy was an important factor to control the size and stability of monomer droplets, if the homogenized energy was insufficient to get the critically stabilized size of monomer droplets, the emulsion was in an unstable region,

droplets would coarsen by Ostwald ripening and monomer diffusion kept going on during the course of polymerization, significant homogeneous/micellar nucleation would be induced. However, in order to achieve the critically stabilized size of droplets, the energy consuming was quite high especially in large scale production and the size of latex particles was limited to smaller values.

In this research, lower homogenization energy was adopted to make the emulsion in an unstable state initially, monomer diffusion would take place, and droplets either coarsen or shrink to lower the overall free energy. After enough equilibrium time, the monomer diffusion was much slower because of approaching or reaching the metastable state, then, the bottom part of emulsion was taken out to undergo further polymerization. Finally, PS latex particles obtained were a one to one copy of the monomer droplets and the size distribution was narrow. The equilibrium time required, importance of costabilizer and initiator were investigated, several parameters would be varied to discuss their effects on particle size. The feature of one-to-one in miniemulsion polymerization was confirmed by comparing the size distributions of monomer droplets and latex particles from dynamic light scattering experiments.

EXPERIMENTAL

Materials

Styrene was distilled under reduced pressure and was stored at 5℃ before use. Hexadecane (HD; Acros), 2,2'-azobisisobutyronitrile (AIBN; Showa), potassium persulfate (KPS; Sigma), sodium dodecyl sulphate (SDS; Acros), polyethylene glycol sorbitan monolaurate (Tween 20; Acros) and cetyltrimethyl ammonium chloride (CTAC; TCI) were used without further purification. Distilled and deionized water was used throughout the work.

Preparation of Latex Particles by Miniemulsion Polymeriazation

All the components required in the experiment were divided into two parts. One was aqueous phase, and the other was oil phase. Aqueous phase was composed of deionized water and surfactant. The surfactant could be anionic (SDS), cationic (CTAC) or nonionic one (Tween 20) in the experiment. Oil phase was composed of styrene, HD and AIBN. All the recipes were listed in Table 1 or Table 2, and the amount of deionized water used was 100g. Being mixed for each for 10min, then the aqueous phase was added to the oil phase and the O/W mixture was mixed for 10min by stirring for pre-emulsification. After that, the O/W mixture was ultrasonicated (Dr. Hielscher UP-50H, 50% amplitude output) in an ice bath for 10min. The use of ice bath was to prevent the polymerization occurring during ultrosonication. Then the homogenized miniemulsion was placed statically for one day in order to redistribute the monomer droplets in a more stable state. Finally, the bottom part of the miniemulsion was taken out by syringe and poured into 250ml four-necked glass reactor equipped with condenser and mechanical stirrer in a water bath. The stirring rate was kept at 300 rpm and polymerization was carried out for 1.5hr at 85℃. If the initiator was KPS, the procedure was the same unless AIBN was removed from oil phase and KPS was introduced to the aqueous phase when polymerization was carried out.

Latex Characterizations

The size and distribution of latex particles were measured by JOEL JEM-1230 transmission electron microscope (TEM). The latex should be diluted with deionized water and was dropped on the surface of cooper grids for observation. The size distributions of monomer droplets and latex particles were obtained by laser dynamic light scattering (DLS) instrument (Malvern Zeta Sizer 3000H). The latex sample was diluted with saturated styrene and surfactant solution with critical micelle concentration (CMC) in order to avoid monomer or surfactant diffusing from droplets to aqueous solution. Each measurement was completed within several minutes, and the size distribution was obtained with particle diameter as horizontal axis and cumulative volume percentage as vertical axis.

RESULT AND DISCUSSIONS

Suitable time for redistribution of monomer droplets into more stable state

In order to determine the suitable equilibrium time for miniemulsion, latex sample, for example S-2, was taken out from the bottom part of homogenized latex at different equilibrium times and the size distribution of monomer droplets was shown in

Fig. 1. It revealed that under low homogenized energy, size of most droplets ranged from 400nm to 550nm initially. However, because the emulsion was in an unstable state, monomer diffusion kept going on, some droplets would shrink and others coarsen by Ostwald ripening. As the equilibrium time was set as 1hr, 3hr, 6hr or 24hr, the size of the shrinking droplets changed to 100-550nm, 100-450nm, 100-200nm and 100-200nm respectively. The shrinking phenomenon was fast in the initial stage and became slower when approaching or achieving the metastable state. Although the change of droplets size was insignificant after 6hr, several factors like temperature or composition could alter the equilibrium time. As a result, 24hr was chosen as a fixed equilibrium time for our further experiment.

Latex particles showing a one to one copy of the monomer droplets

AIBN was the initiator; the concentrations of surfactant and costabilizer were 0.2g and 44mM respectively as shown in Table 1. Anionic surfactant SDS, cationic surfactant CTAC and nonionic surfactant Tween 20 were used respectively to stabilize the O/W surface and the size distributions of droplets and latex particles with different surfactants were shown in Fig. 2. The figure revealed that size distributions of droplets and latex particles were quite similar for each surfactant. It implied that the droplet nucleation was nearly 100% in our system, latex particles showed a one to one copy of the monomer droplets when miniemulsion was situated in a more stable state. The size and distribution of latex particles with different surfactants were also verified by TEM photographs in Fig. 7(a),(b) and (c). When the surfactant was CTAC, the size was smaller and ranged from 100nm to 200nm, otherwise, the size ranged from 130nm~230nm in other surfactants, consistent with the results in our DLS experiment. The difference of the size of final latex particles was ascribed to the nature of surfactant.

Control of size distribution of latex particles by surfactant concentration

The size distribution of miniemulsion was determined by both the processes of droplet fission and fusion [23]. The driving force of droplet fission came from high energy of ultrasonication, and droplet fusion was controlled by combination of droplet coalescence and Ostwald ripening. Higher homogenized energy could enhance the droplet fission and latex particles with smaller size would be obtained[24]. If the droplet fusion was promoted by droplet coalescence or Ostwald ripening, the size of monomer droplets would shift to a larger value[25].

In our experiments, AIBN was the initiator, the concentration of costablizer was 44mM, and the droplet fission was fixed by 10min ultrasonication with 50% amplitude output. The surfactant concentration changed from 3mM, 6mM to 30mM. From the comparison of size distributions of monomer droplets and latex particles with different surfactant concentrations in Fig. 3, the latex particles always showed the one to one copy of monomer droplets and the particle size increased with decreasing the surfactant concentration. The reason of the size changing was that more surfactant could stabilize more O/W surfaces and reduced the possibility of droplet coalescence. As the droplet fusion was retarded by higher concentration of surfactant, the size of droplets would be smaller as expected. TEM photographs in Fig. 7(c),(d) and (e) also verified the results in DLS, when surfactant concentration was from 3mM to 30mM, the range of particle size changed from 110nm-250nm to 60nm-200nm. Moreover, in these three experiments, the size distributions of latex particles were quite narrow when the modified miniemulsion polymerization was used compared with the conventional miniemulsion polymerization.

Was costabilizer necessary for one to one copy the droplets to latex particles?

The initiator we used was AIBN and costabilizer concentration was varied from 0 to 44mM for studying their effects on nucleation mechanism of latex particles. In this series of experiment, the concentration of surfactant, CTAC, was low, 6mM, or high, 30mM. When the surfactant concentration was low, 6mM, the size distributions of monomer droplets and latex particles were shown in Fig. 4. The results revealed that the latex particles showed one to one copy of the monomer droplets as the costabilizer concentration was higher than 8.8mM, it presented that droplet nucleation dominated during polymerization. However, if the costabilizer was absent, two nucleation mechanisms were found and the size distribution of latex particles was in a bimodal shape, the larger ones came from droplet nucleation and the

smaller ones came from homogeneous/micellar nucleation. The results could be confirmed by TEM photographs in Fig.7(c) and (g). In Fig. 7(c), the costabiilzer was 44mM and the size distribution was narrow and ranged from 100nm-200nm. In Fig. 7(g), the costabilizer was absent, larger particles ranged from 100-250nm was one to one copy the monomer droplets and smaller particles with diameter less than 100nm nucleated from micelles or aqueous phase. The results were not surprising according to the Ostwald ripening theory because costabilizer could establish osmotic pressure and hindered the monomer diffusion between droplets with different sizes. Without costabilizer, the one-to-one feature of miniemulsion was partial in the case of lower surfactant concentration. However if the surfactant concentration was higher, the situation changed. Fig. 5 showed the size distributions of monomer droplets and latex particles with or without costabilizer, in which the surfactant concentration used was 30mM, much higher than the previous case of 6mM. The results revealed that almost 100% droplet nucleation was achieved regardless costabilizer was used or not. The TEM photographs in Fig. 7(e) and (f) showed the same results and both size distributions were narrow. For zero costabilizer concentration recipe, HD-4, the size ranged from 100nm-200nm. For 44mM costabilizer concentration recipe, HD-5, the size ranged from 60nm-160nm. The results implied that, the importance of costabilizer was related to the surfactant concentration. The phenomenon could be explained by the stability of droplets. Surfactant and costabilizer both provided the stability for droplets to resist homogeneous/micellar nucleation induced by fluctuation in the course of polymerization. More surfactant could offer better surface coverage of monomer droplets and more costabilizer reduced the Ostwald ripening. As a result, when the costabilzier was absent, the stability provided from surfactant was important. Higher concentration of surfactant could well protect the droplet surfaces and minimize the monomer diffusion out of the droplets during polymerization. These results did not conflict with the principle that the importance of costabilizer was emphasized in most literatures, because most of the miniemulsion polymerization was carried out in a concentration of low surfactant concentration near CMC.

In addition, changing of amount of costabilizer could regulate the size distribution of latex particles. When the concentration of costabilizer was higher, the size distribution would shift to smaller values and DLS data were shown in Fig. 4 and Fig. 5. The results could be explained by the Ostwald ripening theory. Since more costabilizer could reduce the coarsening of monomer droplet and smaller latex particles would be obtained when droplet nucleation was carried out during polymerization.

When water soluble initiator was used

In order to investigate the difference of nucleation mechanism between water soluble initiator and oil soluble initiator during polymerization, size distributions of droplets and latex particles with different initiators were measured and shown in Fig. 6. The surfactant concentration was fixed at 6mM and costabilizer concentration was 44mM.

The sizes of monomer droplets with AIBN as initiator lied in smaller values than those of KPS. The reason was the same as the effect of costabilizer because of the hydrophobic nature of AIBN. It established an osmotic pressure and retarded the coarsening of droplets. As a result, smaller size distribution of droplets was obtained. When the polymerization was carried out, the latex particles showed one to one copy of the monomer droplet as AIBN was used as an initiator. The TEM observation was shown in Fig. 7(c), all latex particles came from droplet nucleation. However significant homogeneous/micellar nucleation would be observed if KPS was used as an initiator. The sizes of latex particles were much smaller than the droplets in KPS system as seen in Fig. 6 and Fig. 7(h). The latex particles were smaller than 100nm in size, which mainly came from homogeneous/micellar nucleation. The results could be ascribed to two reasons. (1) Free radicals from KPS produced in aqueous phase, which enhanced the polymerization of monomer in aqueous phase and particles generated from homogeneous/ micellar nucleation. (2) The size of monomer droplets was larger in KPS system, which was not favorable for droplet nucleation.

CONCLUSION

In this work, a modified miniemulsion polymerization was proposed in order to produce latex particles showing one to one copy of the monomer droplets. The stability of miniemulsion after homogenization depended on the composition and other factors, but it was hard to evaluate before polymerization. If the stability

was poor, monomer diffusion from droplets to droplets would occur and secondary nucleation was induced in the course of polymerization. In our modified process, enough equilibrium time was supplied for the homogenized

miniemulsion. Droplets would redistribute to a more stable state during the time of equilibrium. Better stability of miniemulsion would provide the possibility of 100% droplet nucleation.

Based on the modified process, when AIBN was used as an initiator, after polymerization, the size distribution of latex particles was identical with the monomer droplets no matter the surfactant was anionic, cationic or nonionic, It implied that the latex particles generated from droplet nucleation.

The importance of costabilizer was found to be related to the concentration of surfactant. If the surfactant concentration was low, costabilizer was necessary to carry out an ideal miniemulsion polymerization. If higher surfactant concentration was used, the O/W surfaces were protected well and monomer diffusion among droplets negligible, then latex particles showed one to one copy of the monomer droplets even the costabilizer was absent.

If the initiator was changed from oil soluble to water soluble, the one-to-one feature of miniemulsion polymerization no longer existed. The phenomenon could be ascribed to two reasons. First, KPS increased the polymerization of monomer in aqueous phase and particles mostly generated from homogeneous /micellar nucleation. Second, the size of droplets increased, which was not favorable for the droplet nucleation.

Using this modified process, the size of latex particles could be regulated in a wide ranged from tens of nanometers to hundreds of nanometers. An increase of the amount of surfactant or costabilizer would decrease the size of latex particles. And the size distribution of latex particles remained quite narrow.

REFERENCE

1. Capek I. *Advances in Colloid and Interface Science* 2001;91(2):295-334.
2. Karaman ME, Meagher L, and Pashley RM. *Langmuir* 1993;9(5):1220-1227.
3. Sudol ED and El-Aasser MS. *In Emulsion Polymerization and Emulsion Polymers*, Lovell, P. A.; El-Aasser, M. S., ed. New York: Wiley, 1997.
4. Li CY, Chiu WY, and Lee CF. *E-Polymers* 2007:17.
5. Ando K and Kawaguchi H. *Journal of Colloid and Interface Science* 2005;285(2):619-626.
6. Wormuth K. *Journal of Colloid and Interface Science* 2001;241(2):366-377.
7. Do Amaral M and Asua JM. *Journal of Polymer Science Part a-Polymer Chemistry* 2004;42(17):4222-4227.
8. Blythe PJ, Klein A, Sudol ED, and El-Aasser MS. *Macromolecules* 1999;32(21):6952-6957.
9. Ramirez JC, Herrera-Ordonez J, and Gonzalez VA. *Polymer* 2006;47(10):3336-3343.
10. Antonietti M and Landfester K. *Progress in Polymer Science* 2002;27(4):689-757.
11. Asua JM. *Progress in Polymer Science* 2002;27(7):1283-1346.
12. Taylor P. *Advances in Colloid and Interface Science* 1998;75(2):107-163.
13. Kabalnov AS and Shchukin ED. *Advances in Colloid and Interface Science* 1992;38:69-97.
14. Kabalnov A. *Journal of Dispersion Science and Technology* 2001;22(1):1-12.
15. Bhadra S, Singha NK, and Khastgir D. *Synthetic Metals* 2006;156(16-17):1148-1154.
16. Zhang SW, Zhou SX, Weng YM, and Wu LM. *Langmuir* 2005;21(6):2124-2128.
17. Lim MS and Chen H. *Journal of Polymer Science Part a-Polymer Chemistry* 2000;38(10):1818-1827.
18. Webster AJ and Cates ME. *Langmuir* 1998;14(8):2068-2079.
19. Bechthold N and Landfester K. *Macromolecules* 2000;33(13):4682-4689.
20. Chern CS and Liou YC. *Polymer* 1999;40(13):3763-3772.
21. Jeng J, Dai CA, Chiu WY, and Young PY. *Polymer International* 2007;56(6):746-753.
22. Reimers JL and Schork FJ. *Journal of Applied Polymer Science* 1996;60(2):251-262.
23. Landfester K. *Macromolecular Symposia* 2000;150:171-178.
24. Huang H, Zhang HT, Li JZ, Cheng SY, Hu F, and Tan B. *Journal of Applied Polymer Science* 1998;68(12):2029-2039.
25. Jeng J, Dai CA, Chiu WY, Chern CS, Lin KF, and Young PY. *Journal of Polymer Science Part a-Polymer Chemistry* 2006;44(15):4603-4610.

Table 1. Symbols and recipes for synthesized latex particles with different surfactants

	Styrene (g)	Surfactant (g)	HD (mM)	AIBN (wt%)
CTAC	10	0.2 (6mM)	44	2.5
SDS	10	0.2	44	2.5
Tween 20	10	0.2	44	2.5

The percentage of initiator was based on monomer

The concentration of costabilizer was based on water

Table 2. Symbols and recipes for synthesized latex particles with CTAC as surfactants

	Styrene (g)	Surfactant (mM)	HD (mM)	KPS (wt%)	AIBN (wt%)
S-1	10	3	44	0	2.5
S-2	10	6	44	0	2.5
S-3	10	30	44	0	2.5
HD-1	10	6	0	0	2.5
HD-2	10	6	8.8	0	2.5
HD-3	10	6	44	0	2.5
HD-4	10	30	0	0	2.5
HD-5	10	30	44	0	2.5
AIBN	10	6	44	0	2.5
KPS	10	6	44	0.3	0

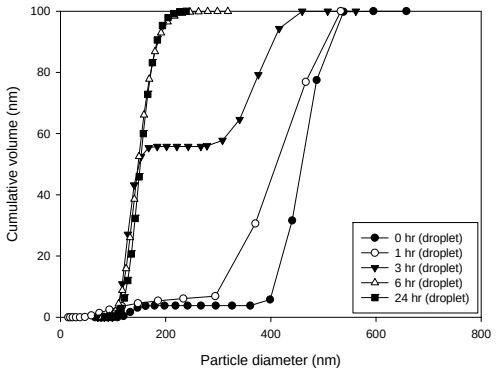

Fig. 1. Size distributions of droplets with different equilibrium times for S-2

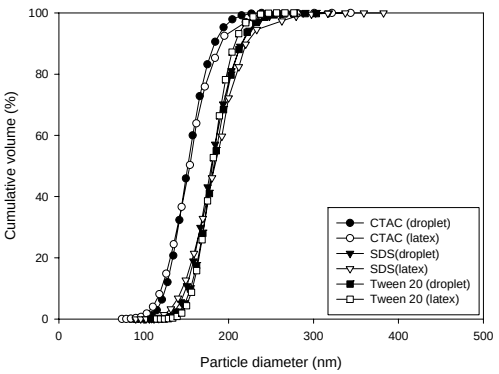

Fig. 2. Size distributions of droplets and latex particles with different surfactants (Recipes were shown in Table 1)

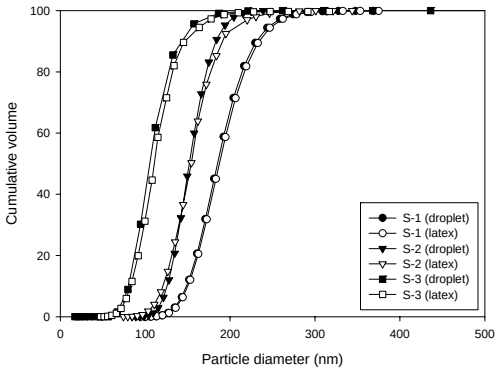

Fig. 3. Size distributions of droplets and latex particles with different amount of surfactant (Recipes were shown in Table 2)

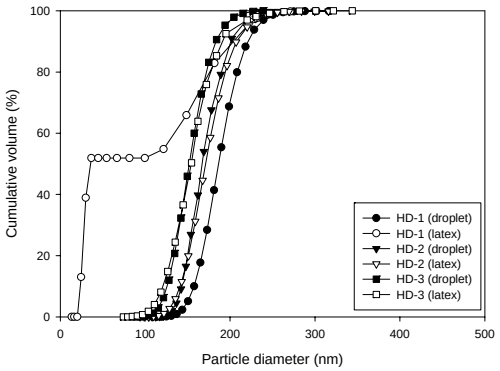

Fig. 4. Size distributions of droplets and latex particles with different amount of costabilizer in lower concentration of surfactant (Recipes were shown in Table 2)

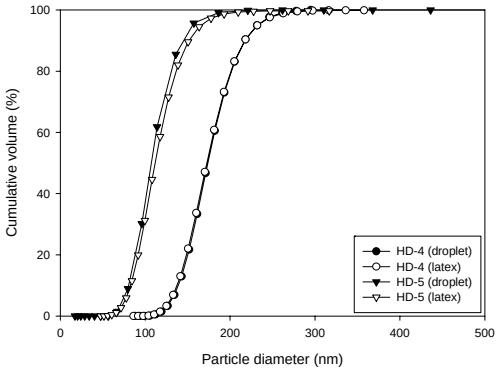

Fig. 5. Size distributions of droplets and latex particles with different amount of costabilizer in higher concentration of surfactant (Recipes were shown in Table 2)

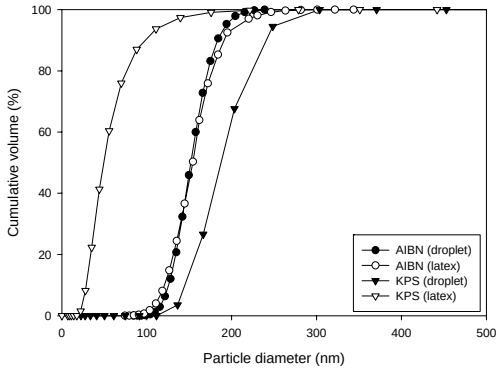

Fig. 6. Size distributions of droplets and latex particles with different initiators (Recipes were shown in Table 2)

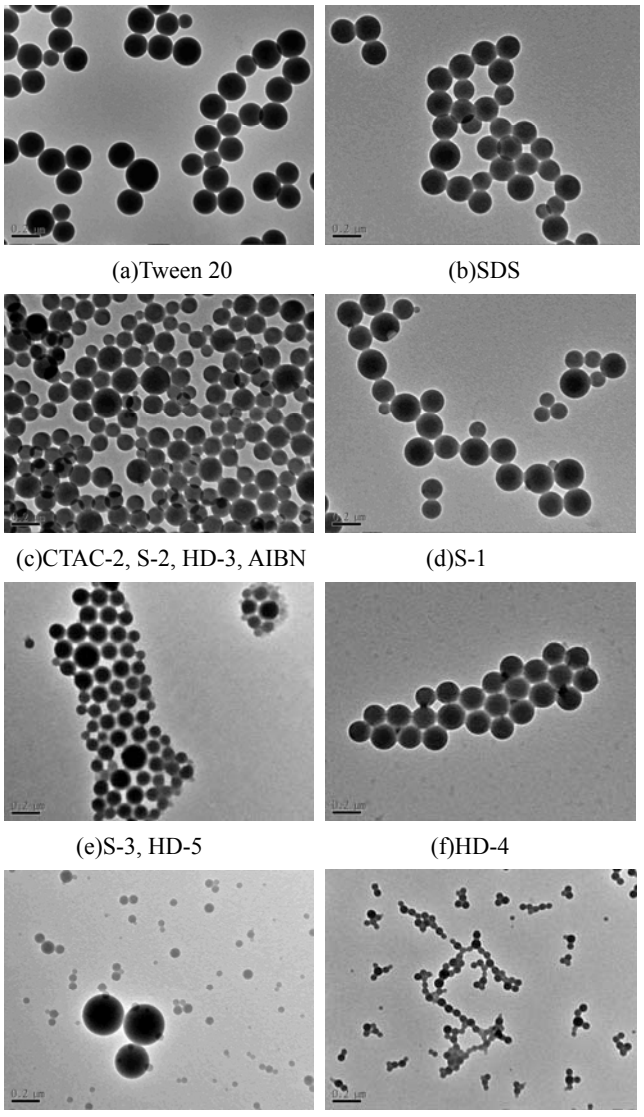

(a)Tween 20 (b)SDS

(c)CTAC-2, S-2, HD-3, AIBN (d)S-1

(e)S-3, HD-5 (f)HD-4

(g)HD-1 (h)KPS

Fig. 7. TEM photographs of synthesized latex particles

PART Ⅱ：Polystyrene/Fe_3O_4 Composite Latex via Miniemulsion Polymerization-Nucleation Mechanism and Morphology

ABSTRACT: In this research, oil-based Fe_3O_4 nanoparticles were prepared by means of coprecipitation method followed by a surface modification using lauric acid. Oil-based Fe_3O_4 could disperse in styrene, and polystyrene/Fe_3O_4(PS/Fe_3O_4) composite particles were prepared via miniemulsion polymerization in the presence of potassium peroxide(KPS) as an initiator, sodium dodecyl sulphate(SDS) as a surfactant, hexadecane(HD) or sorbitan monolaurate(Span 20) as a costabilizer. The effects of Fe_3O_4 content, homogenization energy, amount of initiator, amount of surfactant and costabilizer on the conversion, size distributions of droplets and latex particles, nucleation mechanism and morphology of composite latex particles were investigated. The results showed that different nucleation mechanisms dominated during the course of reaction when polymerization conditions changed. The most important two key factors to influence the nucleation mechanism were homogenization energy and initiator. High homogenization energy provided critically stabilized size of droplets. Otherwise, secondary nucleation, including micellar and/or homogeneous nucleation, would take place rather than droplet nucleation when a water-soluble initiator, KPS, was used. It resulted in two populations of latex particles, pure PS particles in smaller size and PS/ Fe_3O_4 composite particles in larger size.

Keywords: emulsion polymerization, magnetic polymers, particle nucleation, morphology

INTRODUCTION

In recent years, preparation of polymer/inorganic composite particles has attracted much attention. Polymeric particles could be easily prepared and their size and surface groups can be varied in broad range for demand of further application. Polymeric particles also acted as a matrix to disperse and maintain the inorganic particles in a nano domain structure. The function of composite particles could be varied by different inorganic particles applied. They have variety of applications in cosmetics[1,2], paints[3], catalyst[4] and biochemistry[5,6]. For example, the magnetic property of Fe_3O_4 and catalytic activity property of TiO_2 were widely well known and useful, and the inorganic particles could be coated on the polymer surface or be encapsulated in the interior of polymer matrix. Among variety of composite particles, magnetic polymer particles have been investigated enormously because of their diversified applications in cell separation[7], food analysis[8] and targeting drug delivery[9,10].

For magnetic polymer particles, a variety of encapsulation techniques have been developed including conventional emulsion polymerization[11-14], precipitation polymerization[15], suspension polymerization[16], seeded polymerization[17-18], soapless emulsion polymerization[19,20], miniemulsion polymerization[21-23], and so on[24,25]. Wang et al.[17] synthesized magnetic PMMA composite latex particles by seeded emulsion polymerization and found two nucleation mechanisms involved according to the polymerization conditions. In the monomer-rich and less ferrofluid system, self-nucleation of PMMA was dominant. In the ferrofluid-rich system, seeded emulsion polymerization was the main course to form the magnetic composite latex particles. Pich et al.[19] encapsulated iron oxide in poly(styrene/acetoacetoxyethyl methacrylate) by surfactant free polymerization and the encapsulation degree was higher when iron oxide was undergone surface modification by sodium oleate. Variation of monomer to iron oxide ratio gave a possibility to change morphology.

In recent literature, miniemulsion polymerization was regarded as an effective method to obtain polymer/inorganic composite particles because of the characteristic feature, named droplet nucleation. In miniemulsion, the size of monomer droplets ranged from 50 to 500nm, adjusted by changing the amount of surfactant or costabilizer, solid content and homogenization energy[26,27]. Contrary to conventional emulsion polymerization, the nucleation and propagation site was not in water or micelles, monomer droplets would directly convert to particles, so the size distribution of droplets and its corresponding latex particles were identical[28,29]. However, no matter what kind of polymerization method was used, including miniemulsion polymerization, most of the researches in literature emphasized the preparation and characterization of magnetic polymer particles. There were few papers discussing the morphology and nucleation mechanism in polymer/inorganic composite particles. The aim of this paper was to investigate the nucleation mechanism and polymerization kinetics through the course of miniemulsion polymerization in the presence of

magnetic particles. In the meanwhile, parameters which could tune the morphology of PS/Fe_3O_4 composite particles would also be discussed.

EXPERIMENTAL

Materials

Styrene was distilled under reduced pressure and was stored at 5℃ before use. Hexadecane(HD; Acros), 2,2'-azobisisobutyronitrile (AIBN; Showa), potassium peroxide (KPS; Sigma), dodecyl sulphate (SDS; Acros), lauric acid(Acros), sorbitan monolaurate (Span 20; Showa) and 28% ammonium hydroxide solution(Acros) were used without further purification. Distilled and deionized water was used throughout the work.

Preparation of Oil-Based Fe_3O_4 Particles

Fe_3O_4 particles were obtained by coprecipitation of Fe(Ⅱ) and Fe(Ⅲ) salts in aqueous solution of ammonium hydroxide. In this process, 23.5g $FeCl_3 \cdot 6H_2O$ and 8.6g $FeCl_2 \cdot 4H_2O$ were dissolved in 400ml deionized water with stirring. Then 50ml of 28%(w/w) ammonium hydroxide solution was added for 6min. Further 2.5g lauric acid was added to the solution under stirring at 90℃ for 30min to modify the surfaces of Fe_3O_4 particles to become hydrophobic in nature. Finally, the supernatant solution was decanted and the black modified Fe_3O_4 residue was washed with methanol for three times to remove non-bonded lauric acid. Then the precipitates were lyophilized for 24hr to obtain oil-base Fe_3O_4 particles.

Preparation of PS/Fe_3O_4 Composite Particles by Miniemulsion Polymeriazation

All the components required in the experiment were divided into three parts. One was aqueous phase, one was oil phase and the other was initiator solution. Aqueous phase was composed of deionized water and SDS, oil phase was composed of styrene, Fe_3O_4 and HD, and initiator solution was composed of deionized water and KPS. All the recipes were listed in Table 1 and the amount of deionized water used was 100g. Being mixed for each for 10min, then the aqueous phase was added to the oil phase and the O/W mixture was mixed for 10min by mechanical stirring for pre-emulsification. After that, the O/W mixture was ultrasonicated (Dr. Hielscher UP-50H) in an ice bath. The ultrasonication time and amplitude were two parameters discussed in the experiment and the use of ice bath was to prevent the polymerization occurring during ultrosonication. Finally the homogenized miniemulsion was poured into 250ml four-necked glass reactor equipped with condenser and mechanical stirrer in a water bath. The stirring rate was kept at 300 rpm and polymerization was carried out by introducing initiator solution for 1hr at 85℃

Conversion

The conversion of monomer was determined by gravimetric method. During miniemulsion polymerization, certain amount of the latex was taken out of the reactor, and poured into a hydroquinone methanol solution in an ice bath. Finally, the sample was dried in an oven at 85℃ until the weight kept constant. The conversion can be calculated by eq(1). P was the weight of dry sample from the oven. F was the theoretical weight of Fe_3O_4 in the dry sample. W was the weight of the latex sample and M_0 was the weight fraction of monomer in feed recipes.

$$Conversion = \frac{P - F}{W \times M_0} \times 100\% \quad (1)$$

Morphology of PS/Fe_3O_4 Composite Particles

The PS/Fe_3O_4 composite latex was diluted with deionized water. Then the sample was dropped on the surface of cooper grids, the morphology and particles size could be observed by using JOEL JEM-1230 transmission electron microscope (TEM)

Size Distributions of Monomer Droplets and Composite Latex Particles

The size distribution of the monomer droplets or composite latex particles was measured by laser dynamic light scattering (DLS) instrument (Malvern Zeta Sizer 3000H). The latex sample was diluted with saturated styrene and SDS solution in order to avoid monomer or SDS diffusing from droplets to aqueous solution. Each measurement was completed within several minutes, and the size distribution was obtained with particle diameter as horizontal axis and cumulative volume percentage as vertical axis.

RESULTS AND DISCUSSION

Effect of Content of Fe_3O_4

Size distributions of monomer droplets and latex particles with

different Fe_3O_4 contents were showed in Figure 1. The result showed that, in Fe-2, with 20% Fe_3O_4, the size distribution of droplets was broad and ranged from 200nm to 500nm. For Fe-1, with 10% Fe_3O_4, the distribution of droplet size shifted to smaller values, 170nm to 350nm, and for Fe_3O_4 free system, Fe-0, 60% of the droplets had diameter less than 200nm. It revealed that Fe_3O_4 dispersed in monomer would reduce the efficiency of droplet fission during ultrasonication and resulted in broader size distribution and larger average diameter of droplets. After polymerization, Fe-1 and Fe-2 both had bimodal particle size distribution, the larger particles mainly formed from the shrinking of original droplets, and the smaller particles mainly came from secondary nucleation. For Fe-0, unimodal particle size distribution was obtained and most latex particles produced from secondary nucleation. From the comparison of size distributions of droplets and latex particles in these three experimental conditions, large population of particles formed from secondary nucleation.

Conversion curves with different amounts of Fe_3O_4 were shown in Figure 2, when the content of Fe_3O_4 increased, the polymerization rate was higher in the middle stage of polymerization, but the limiting conversion was significantly lower. As discussed in Figure 1, the size of polymer particles and the viscosity in polymer particles increased as the content of Fe_3O_4 increased. These two situations might induce both significant autoacceleration in the middle stage of polymerization and diffusion-controlled propagation in the final stage of polymerization. In other words, as the content of Fe_3O_4 increased in the reaction system, the higher polymerization rate was due to the autoacceleration and the lower limiting conversion was due to the diffusion-controlled propagation.

TEM photographs of the obtained composite particles were shown in Figure 3. The results were consistent with the particle size distribution curves from dynamic light scattering experiment. Two groups of particles were found, one was pure polymer particles in small size and the other was composite particles in large size. With more content of Fe_3O_4, the size of larger composite latex particles increased, because the larger original droplets resulted in larger composite particles even after shrinking. However changing the Fe_3O_4 content did not change the morphology of composite particles and core-shell composite particles were observed with Fe_3O_4 on the shell. The formation of core-shell structure with Fe_3O_4 on the shell was ascribed to the significant occurrence of secondary nucleation. Fe_3O_4 were taken out to the surfaces of particles as styrene diffused out from droplets to aqueous solution for the need of secondary nucleation.

Effect of homogenization energy

The homogenization energy applied to the O/W emulsion could be varied by adjusting the ultrasonication time and amplitude, the longer ultrasonication time and higher ultrasonication amplitude reflected more energy. From Figure 4, when homogenization energy applied increased from Energy-1 to Energy-3, the distribution of droplets would become narrower and the average particle size shifted to a smaller value. Furthermore, from the comparison of size distributions of initial droplets and latex particles, the size difference was obvious especially in Energy-1. It was because that the critically stabilized size of droplets was not achieved in the case of low homogenization energy and the possibility of droplet nucleation largely decreased. Although droplet nucleation was not the main course throughout the polymerization in these three experimental conditions, but we still could conclude that, higher homogenization energy could produce more and smaller droplets and increased the opportunity of droplet nucleation.

In Figure 5, the conversion curves of the composite latex showed that as increasing the homogenization energy, the polymerization rate would be promoted. It appeared that more energy applied to the O/W emulsion, the monomer would split into more small droplets. In other words, during polymerization, the reaction sites for droplet nucleation increased and the polymerization rate was enhanced.

TEM photographs of the synthesized composite latex particles were shown in Figure 6 for Energy-3 and in Figure 3(b) for Energy-1. The results showed that the morphology of composite particles was in core-shell structure with Fe_3O_4 on the shell. Moreover, as increasing the homogenization energy during ultrasonication, the relative amount of Fe_3O_4 containing latex particles was higher owning to more tendency of droplet nucleation.

Effect of amount of initiator

From the comparison of size distributions of droplets and latex

particles with different amount of initiator in Figure 7, it indicated the nucleation mechanism was dominated by secondary nucleation according to emergence of numerous particles smaller than original monomer droplets regardless the amount of initiator used. Nevertheless, size distributions of latex particles were quite different, when amount of initiator increased from 0.3wt% to 2.5wt%, the distribution became broader and larger particles were observed. It could be attributed to the higher ionic strength, induced by water soluble initiator, which resulted in compression of electrical double layer. Therefore, the stability of particles was decreased and coagulation occurred during polymerization.

The conversion curves with different amount of initiator were showed in Figure 8, it revealed that polymerization rate was enhanced as the amount of initiator increased. As expected, free radicals were generated from initiator, and more free radicals participated in polymerization guaranteed faster reaction. However, the final conversion was highly limited when amount of initiator was up to 2.5wt%. This phenomenon could be explained by diffusion-controlled propagation. In the course of polymerization, T_g of polymer/monomer mixture in polymer particles increased. As long as the T_g of polymer particles was higher than the polymerization temperature, mobility of free radicals was hindered and the diffusion-controlled propagation was obvious especially in larger particles in I-3. Therefore, polymerization might stop and a limiting conversion was observed significantly decreased with increasing the initiator concentration.

TEM photographs of I-1 and I-3 were showed in Figure 6 and Figure 9. The morphology of PS/Fe_3O_4 latex particles could be varied with particle coagulation. In less coagulation recipe, I-1, the location of Fe_3O_4 was on the shell of particles. However, for I-3, Fe_3O_4 particles were most located in the interior of particles due to the coagulation of particles.

Effect of amount of surfactant

The function of surfactant, SDS, was to keep the droplets or polymer particles from coalescence and provided enough electrostatically repulsive force to maintain the stability of monomer droplets or polymer particles. From the comparison of size distributions of droplets and latex particles with different amount of surfactant in Figure 10, the size of monomer droplets was in the order of SDS-3< SDS-2< SDS-1. When the amount of surfactant increased, monomer would split into smaller and more droplets during the process of ultrasonication. After polymerization, the size distribution of latex particles revealed that if the concentration of surfactant was 35mM, little coagulation was observed; if 20mM, particle coagulation was very significant and the size of polymer particles were larger than the original sizes of droplets. That was because the amount surfactant was insufficient to provide enough stability for droplets or polymer particles. Figure 11 showed the conversion curves with different surfactant concentration, the polymerization rate was in the order of SDS-3> SDS-2>SDS-1. It could be ascribed to that small monomer droplets acted as reaction loci and polymerization rate increased with increasing the number of droplets, and the average size of composite particles decreased.

Furthermore, compared the TEM photographs of SDS-2 and SDS-3 (shown in Figure 12 and Figure 6), in SDS-3, the location of Fe_3O_4 particles was on the shell of particles. However, for SDS-2, some Fe_3O_4 particles were located in the interior of particles. Like I-2, the change of morphology was caused by particle coagulation.

Effect of costabilizer

The role of costabilizer was to suppress molecular diffusion (Oswald ripening effect) by introducing osmotic pressure and maintain the droplet stability under polymerization. In this series of experiment, HD and Span 20 were chosen as two types of costabilizer where HD was a highly hydrophobic compound and Span 20 was relatively more hydrophilic due to its shorter hydrocarbon chain and three hydrophilic hydroxyl functional groups. Due to the amphiphilic nature of Span 20, it can also be used as a surfactant. Compared with the size distributions of droplets and latex particles in Figure 13, the average diameter of latex composite particles was smaller than droplets regardless what kind of costabilizers was used. It implied that particles formed from both secondary nucleation and droplet nucleation. Moreover, because of the surfactant role of Span 20, the coagulation could be avoided to some extent, thus the particles were obtained with smaller size.

Conversion curves of HD-1 and Span-1 were shown in Figure 14. When costabilizer was changed from HD to Span 20, the polymerization rate was accelerated. It was because that Span 20

acted not only a costabilizer but also a surfactant. More surfactant was available to stabilize the O/W surfaces during ultrasonication, the number of monomer droplets as reaction site increased, therefore, the polymerization rate increased.

The morphology of composite latex particles with different costabilizer was observed by TEM photographs in Figure 12 and Figure 15. The location of Fe_3O_4 was on the shell of particles if using Span 20 as a costabilizer in Figure 15, in a less coagulation situation. On the other hand, if coagulation was significant as in the case of Figure 12, Fe_3O_4 particles were located more in the interior of particles

Effect of initiator on nucleation mechanism

In order to investigate the difference of nucleation mechanism between water soluble initiator and oil soluble initiator during polymerization, size distributions of droplets and latex particles with different initiator were measured and shown in Figure 16. The results showed that, when AIBN was used as an initiator, the size distributions of droplets and latex particles were very similar, indicating droplet nucleation was the main route in the course of polymerization. However, if KPS was used as an initiator, after polymerization, latex particles with bimodal distribution would be obtained, the smaller particles came from secondary nucleation, and the larger ones came from droplet nucleation and coagulation of particles. As a result, we can conclude that, using AIBN as an initiator could largely decrease the possibility of secondary nucleation. The less opportunity for radicals existing in aqueous solution was the key reason to depress secondary nucleation.

TEM photographs of latex particles with different conversions were taken. Figure 17(a)-(c) showed the morphology of latex particles initiated by KPS with conversions 3%, 32% and 52% respectively. Two populations were observed. Smaller particles were pure polymer particles coming from secondary nucleation; the size was uniform and increased slightly with increasing the conversion. On the other hand, larger particles were composite particles coming from droplet nucleation and coagulation, their sizes increased slightly with conversion too. Finally, from the TEM photograph of latex particles initiated by AIBN in Figure 17(d), Fe_3O_4 containing latex particles were mainly observed. The droplet nucleation dominated during polymerization with AIBN as an initiator, while both droplet nucleation and secondary nucleation were important in the polymerization system with KPS as an initiator, consistent with the finding from DLS experiment.

CONCLUSION

In this work, PS/Fe_3O_4 composite particles were synthesized successfully by miniemulsion polymerization. The conversion curves, size distributions of droplets and latex particles, nucleation mechanism and morphology were discussed in detail. Polymerization rate could be promoted by introducing more free radicals during polymerization via higher initiator concentration or increasing the number of monomer droplets, which could be achieved under the condition of high concentration of surfactant, higher homogenization energy or changing costabilizer form HD to Span 20.

The size distributions of droplets and latex particles were measured and compared to estimate the relative importance of droplet nucleation. With increasing the Fe_3O_4 content, the size distributions of droplets and latex particles were broader with more population of larger particles due to the less efficiency of droplet fission during ultrasonication. Under high homogenization energy, the monomer droplets were critically stabilized and the difference of size distributions between monomer droplets and latex particles decreased. The function of SDS was to provide stabilization for O/W surfaces, insufficient amount of surfactant could not maintain the stability of monomer droplets and coagulation of particles could not be avoided during polymerization. In addition, because of the surfactant role of Span 20, changing the costabilizer from HD to Span 20 increased the stability of monomer droplets and prevented particles from coagulation. When using KPS as an initiator, secondary nucleation dominated in the course of polymerization even though the critically stabilized size of droplets was achieved by high homogenization energy. If AIBN was used as an initiator, droplet nucleation dominated and the fraction of secondary nucleation was largely reduced, in the meanwhile encapsulation degree of PS/Fe_3O_4 latex particles was better.

Morphology of composite latex particles could be varied with the particle coagulation during polymerization. Increasing the amount of initiator, or decreasing the amount of surfactant, coagulation of droplets and particles was more serious and Fe_3O_4 would be incorporated into the interior of particles. Otherwise,

Fe_3O_4 would be located on the surfaces of particles, and core-shell structure of composite particles was observed.

REFERENCE

1. Tang, E. J.; Cheng, G. X.; Pang, X. S.; Ma, X. L.; Xing, F. B. *Colloid Polym Sci* 2006, **284**, 422-428.
2. Kim, J. W.; Shim, J. W.; Bae, J. H.; Han, S. H.; Kim, H. K.; Chang, I. S.; Kang, H. H.; Suh, K. D. *Colloid Polym Sci* 2002, **280**, 584-588.
3. Mizutani, T.; Arai, K.; Miyamoto, M.; Kimura, Y. *Prog Org Coat* 2006, **55**, 276-283.
4. Chen, C. W.; Serizawa, T.; Akashi, M. *Chem Mat* 1999, **11**, 1381-1389.
5. Zheng, W. M.; Gao, F.; Gu, H. C. *J. Magn Magn Mater* 2005, **293**, 199-205.
6. Wang, P. C.; Lee, C. F.; Young, T. H.; Lin, D. T.; Chiu, W. Y. *J Polym Sci Part A: Polym Chem* 2005, **43**, 1342-1356.
7. Haik, Y.; Pai, V.; Chen, C. J. *J. Magn Magn Mater* 1999, **194**, 254-261.
8. Pyle, B. H.; Broadaway, S. C.; McFeters, G. A. *Appl Environ Microbiol* 1999, **65**, 1966-1972.
9. Alexiou, C.; Schmid, R. J.; Jurgons, R.; Kremer, M.; Wanner, G.; Bergemann, C.; Huenges, E.; Nawroth, T.; Arnold, W.; Parak, F. G. *Eur Biophys J Biophys Lett* 2006, **35**, 446-450.
10. Alexiou, C.; Jurgons, R.; Schmid, R. J.; Bergemann, C.; Henke, J.; Erhardt, W.; Huenges, E.; Parak, F. *J Drug Target* 2003, **11**, 139-149.
11. Pollert, E.; Knizek, K.; Marysko, M.; Zaveta, K.; Lancok, A.; Bohacek, J.; Horak, D.; Babic, M. *J. Magn Magn Mater* 2006, **306**, 241-247.
12. Xie, G.; Zhang, Q. Y.; Luo, Z. P.; Wu, M.; Li, T. H. *J Appl Polym Sci* 2003, **87**, 1733-1738.
13. Horak, D.; Chekina, N. *J. Appl Polym Sci* 2006, **102**, 4348-4357.
14. Lee, C. F.; Chou, Y. H.; Chiu, W. Y. *J Polym Sci Part A: Polym Chem* 2007, **45**, 3062-3072.
15. Mackova, H.; Horak, D. *J Polym Sci Part A: Polym Chem* 2006, **44**, 968-982.
16. Wang, X. B.; Ding, X. B.; Zheng, Z. H.; Hu, X. H.; Cheng, X.; Peng, Y. X. *Macromol Rapid Commun* 2006, **27**, 1180-1184.
17. Wang, P. C.; Chiu, W. Y.; Lee, C. F.; Young, T. H. *J Polym Sci Part A: Polym Chem* 2004, **42**, 5695-5705.
18. Montagne, F.; Mondain-Monval, O.; Pichot, C.; Elaissari, A. J Polym Sci Part A: Polym Chem 2007, 45, 3062-3072.
19. Pich, A.; Bhattacharya, S.; Ghosh, A.; Adler, H. J. P. *Polymer* 2005, **46**, 4596-4603.
20. Faridi-Majidi, R.; Sharifi-Sanjani, N.; Agend, F. *Thin Solid Films* 2006, **515**, 368-374.
21. Liu, X. Q.; Guan, Y. P.; Ma, Z. Y.; Liu, H. Z. *Langmuir* 2004, **20**, 10278-10282.
22. Csetneki, I.; Faix, M. K.; Szilagyi, A.; Kovacs, A. L.; Nemeth, Z.; Zrinyi, M. *J Polym Sci Part A: Polym Chem* 2004, **42**, 4802-4808.
23. Zheng, W. M.; Gao, F.; Gu, H. C. *J Magn Magn Mater* 2005, **288**, 403-410.
24. Vestal, C. R.; Zhang, Z. J. *J Am Chem Soc* 2002, **124**, 14312-14313.
25. Wu, T. M.; Yen, S. J.; Chen, E. C.; Sung, T. W.; Chiang, R. K. *J Polym Sci Part A: Polym Chem* 2007, **45**, 3062-3072.
26. Asua, J. M. *Prog Polym Sci* 2002, **27**, 1283-1346.
27. Antonietti, M.; Landfester, K. *Prog Polym Sci* 2002, **27**, 689-757.
28. Landfester, K.; Bechthold, N.; Tiarks, F.; Antonietti, M. *Macromolecules* 1999, **32**, 2679-2683.
29. Landfester, K.; Bechthold, N.; Forster, S.; Antonietti, M. *Macromol Rapid Commun* 1999, **20**, 81-84.

Table 1. Symbols and Recipes for Synthesized Composite Particle

	Fe_3O_4 (%)	SDS (mM)	Costabilizer	Energy	KPS (wt%)	AIBN (wt%)
Fe-0	0	70	HD	50% 13min	0.3	0
Fe-1	10	70	HD	50% 13min	0.3	0
Fe-2	20	70	HD	50% 13min	0.3	0
Energy-1	10	70	HD	50% 13min	0.3	0
Energy-2	10	70	HD	50% 30min	0.3	0
Energy-3	10	70	HD	100% 30min	0.3	0
SDS-1	10	20	HD	100% 30min	0.3	0
SDS-2	10	35	HD	100% 30min	0.3	0
SDS-3	10	70	HD	100% 30min	0.3	0
I-1	10	70	HD	100% 30min	0.3	0
I-2	10	70	HD	100% 30min	1	0
I-3	10	70	HD	100% 30min	2.5	0
HD-1	10	35	HD	100% 30min	0.3	0
Span-1	10	35	Span 20	100% 30min	0.3	0
KPS	10	35	HD	100% 30min	0.3	0
AIBN	10	35	HD	100% 30min	0	2.5

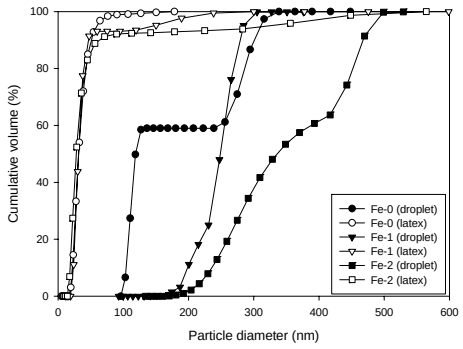

Figure 1. Size distributions of droplets and latex particles with different amount of Fe_3O_4

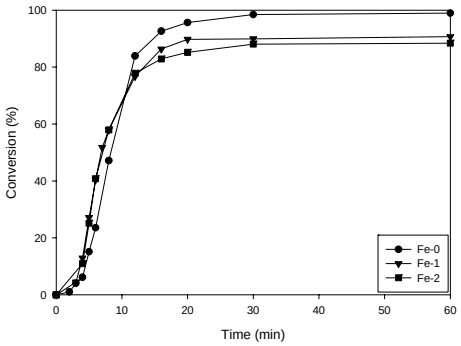

Figure 2. Monomer conversion versus time with different amount Fe_3O_4

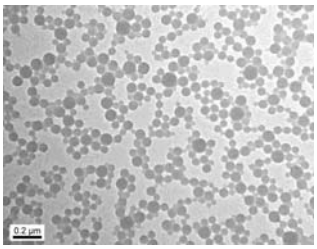

(a)Fe-0

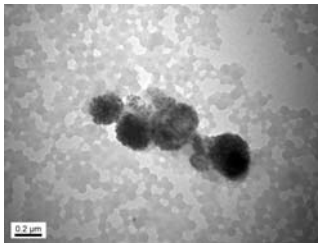

(b)Fe-1,Energy-1

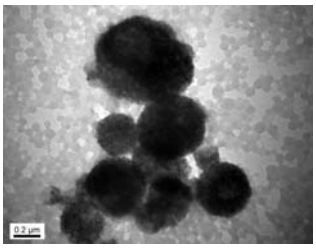

(c)Fe-2

Figure 3. TEM photographs of synthesized composite latex particles with different amount of Fe_3O_4

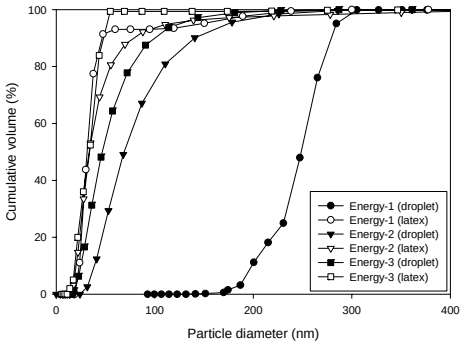

Figure 4. Size distributions of droplets and latex particles with different homogenized energy

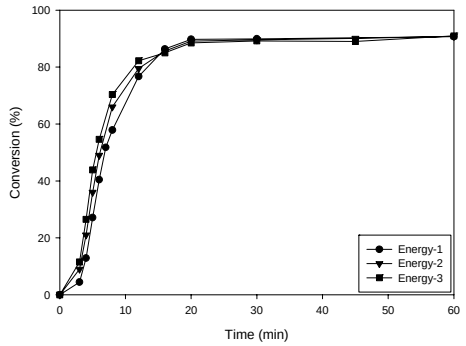

Figure 5. Monomer conversion versus time with different homogenized energy

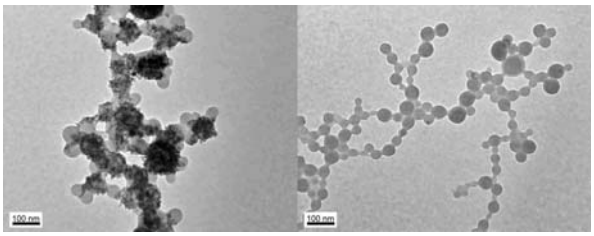

Figure 6. TEM photographs of synthesized composite latex particles SDS-3 , I-1 , Energy-3

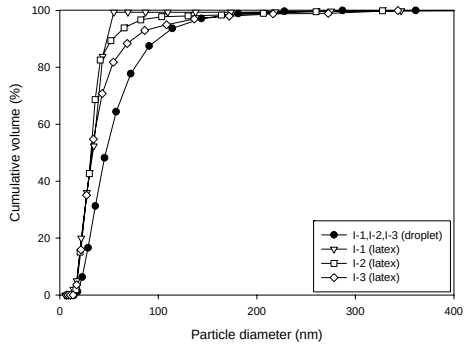

Figure 7. Monomer conversion versus time with different amount of initiator

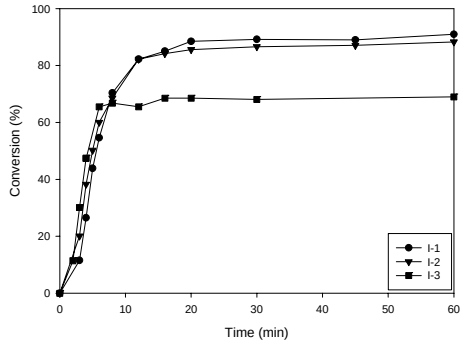

Figure 8. Monomer conversion versus time with different amount of initiator

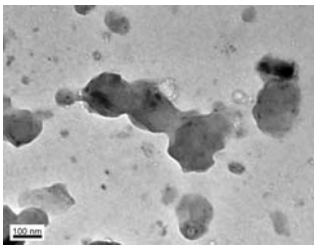

Figure 9. TEM photographs of synthesized composite latex particles I-3

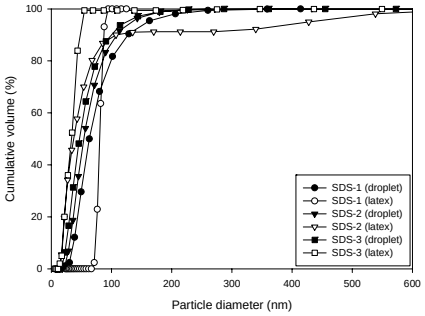

Figure 10. Size distributions of droplets and latex particles with different amount of surfactant

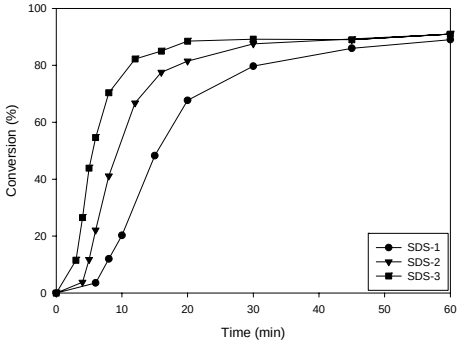

Figure 11. Monomer conversion versus time with different amount of surfactant

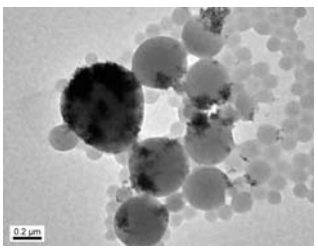

Figure 12. TEM photographs of synthesized composite latex particles SDS-2 , HD-1

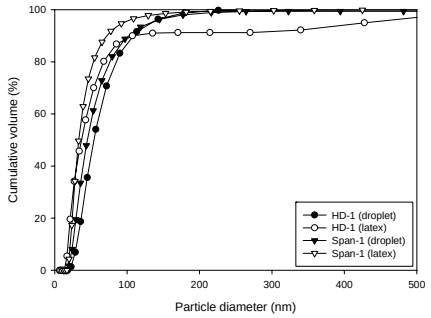

Figure 13. Size distributions of droplets and latex particles with different costabilizer

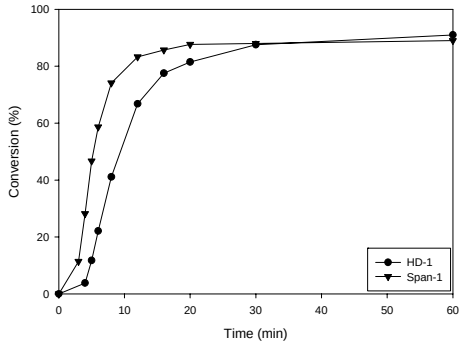

Figure 14. Monomer conversion versus time with different costabilizer

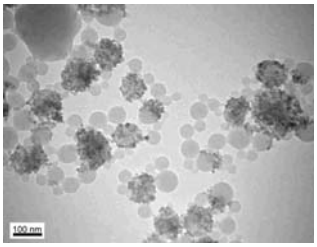

Figure 15. TEM photographs of synthesized composite latex particles Span-1

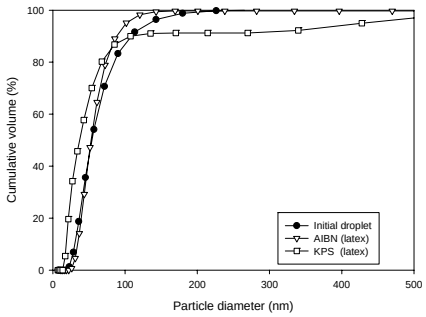

Figure 16. Size distributions of droplets and latex particles with different initiator

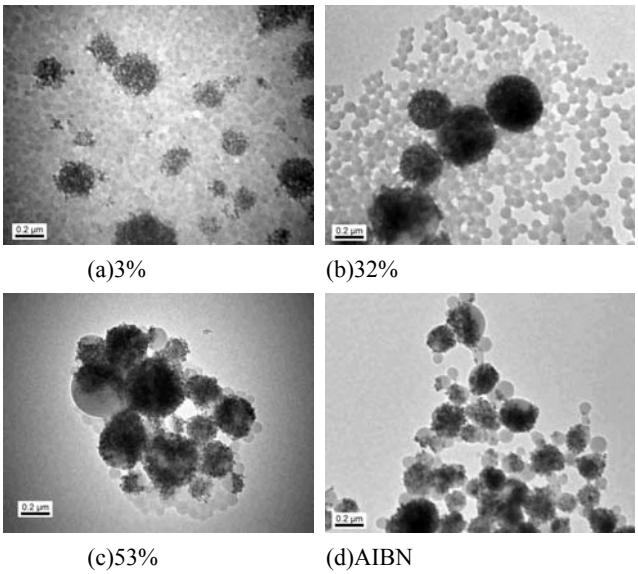

Figure 17. TEM photographs of synthesized composite particles using KPS as initiator with different conversion or using AIBN as initiator

PARTⅢ：Nucleation Mechanism and Morphology of Composite Latex Particles, Polystytrene/Fe_3O_4, via Miniemulsion Polymerization using AIBN as Initiator

ABSTRACT: In this research, oil-based Fe_3O_4 nanoparticles were prepared by means of coprecipitation method followed by a surface modification using lauric acid. Oil-based Fe_3O_4 could disperse in styrene, and polystyrene/Fe_3O_4(PS/Fe_3O_4) composite particles were prepared via miniemulsion polymerization in the presence of 2,2'-azobisisobutyronitrile(AIBN) as initiator, sodium dodecyl sulphate(SDS) as surfactant, hexadecane(HD) or sorbitan monolaurate(Span 20) as costabilizer. The effects of Fe_3O_4 content, costabilizer, homogenization energy and surfactant concentration on the conversion, size distributions of droplets and latex particles, nucleation mechanism and morphology of composite particles were investigated. The results showed that high homogenization energy, appropriate amount of SDS and more hydrophobic costabilizer were necessary to obtain composite particles from droplet nucleation. Morphology of magnetic composite particles could be well controlled by homogenization energy or hydrophobicity of costabilizer. Fe_3O_4 nanoparticles could be located inside latex particles or on the shell of latex particles depending on the polymerization conditions.

Keywords: miniemulsion polymerization, nucleation mechanism, magnetic latex particles, morphology

INTRODUCTION

In the past few years, magnetic polymer composite particles have drawn more and more attention due to vast applications in several fields, such as cell separation[1,2], enzyme immobilization[3], environment and food analysis[4], magnetic resonance imaging[5] and targeting drug delivery[6,7]. The popularity was caused by its sensitivity to magnetic filed applied and could be separated easily by magnetic separation.

Many polymerization methods have been developed to prepare magnetic polymer composite particles, including conventional emulsion polymerization[8], precipitation polymerization[9] suspension polymerization[10], seeded polymerization[11], soapless emulsion polymerization[12], miniemulsion polymerization[13-17], and so on[18]. In the method of miniemulsion polymerization, magnetic particles were undergone surface modification using organic acid, where carboxyl functional group would anchor on the iron atom[19], and dispersed into the monomer, then, the monomer droplets with magnetic particles would act as nanoreactors and polymerization proceeded in situ. Lu et al.[15] examined the effects of the experiment parameters on the encapsulation degree of magnetic PS composite particles, such as surfactant concentration, hydrophobe concentration, stabilizer and comonomer concentration. Ramirez and Landfester[16] synthesized magnetic polystyrene particles with high magnetite content successfully and developed a new three-step miniemulsion preparation route. Lin et al.[17] produced thermoresponsive magnetic composite particles, with Fe_3O_4 homogeneously distributed in NIPAAm, via W/O miniemulsion polymerization.

As miniemulsion polymerization was widely taken as an effective method to prepare polymer/inorganic composite particles. Besides Fe_3O_4, there were other inorganic particles have been tried and investigated. Erdem et al.[20] produced TiO_2/PS composite particles and described the encapsulation efficiency using hydrophilic or hydrophobic TiO_2 particles in the presence of OLOA 370 as stabilizer. Peres et al.[21] produced green-emitting CdSe/poly(butyl acrylate) nanocomposite particles and investigated the morphology and electrical property. In additional, carbon black/PS[22], ZnO/BA[23] and $CaCO_3$/PS[24] composite particles were also obtained by miniemulsion polymerization. However, no matter what the polymerization method or inorganic material were used, most of the researches in literature emphasized the preparation and characterization, especially in miniemulsion polymerization. There were few papers discussing the control of morphology and nucleation mechanism in polymer/inorganic composite particles.

The aim of this paper was to examine how polymerization conditions affected the morphology of PS/Fe_3O_4 composite particles, in the meanwhile, nucleation mechanism and polymerization kinetics through the course of miniemulsion polymerization in the presence of magnetic particles would also be discussed.

EXPERIMENTAL

Materials

Styrene was distilled under reduced pressure and was stored at 5℃ before use. Hexadecane (HD; Acros), 2,2'-azobisisobutyronitrile (AIBN; Showa), sodium dodecyl sulphate (SDS; Acros), lauric acid(Acros), sorbitan monolaurate (Span 20; Showa) and 28% ammonium hydroxide solution(Acros) were used without further purification. Distilled and deionized water was used throughout the work.

Preparation of Oil-Based Fe_3O_4 Particles

Fe_3O_4 particles were obtained by coprecipitation of Fe(Ⅱ) and Fe(Ⅲ) salts in aqueous solution of ammonium hydroxide. In this process, 23.5g $FeCl_3 \cdot 6H_2O$ and 8.6g $FeCl_2 \cdot 4H_2O$ were dissolved in 400ml deionized water with stirring. Then 50ml of 28%(w/w) ammonium hydroxide solution was added for 6min. Further 2.5g lauric acid was added to the solution under stirring at 90℃ for 30min to modify the surfaces of Fe_3O_4 particles to become hydrophobic in nature. Finally, the supernatant solution was decanted and the black modified Fe_3O_4 residue was washed with methanol for three times to remove non-bonded lauric acid. Then the precipitates were lyophilized for 24hr to obtain oil-base Fe_3O_4 particles.

Preparation of PS/Fe_3O_4 Composite Particles by Miniemulsion Polymeriazation

All the components required in the experiment were divided into two parts. One was aqueous phase and the other was oil phase. Aqueous phase was composed of deionized water and SDS, oil phase was composed of styrene, Fe_3O_4, HD and AIBN. All the recipes were listed in Table 1 and the amount of deionized water used was 100g. Being mixed for each for 10min, then the aqueous phase was added to the oil phase and the O/W mixture was mixed for 10min by mechanical stirring for pre-emulsification. After that, the O/W mixture was ultrasonicated (Dr. Hielscher UP-50H) in an ice bath. The ultrasonication time and amplitude were two parameters discussed in the experiment and the use of ice bath was to prevent the polymerization occurring during ultrosonication. Finally the homogenized miniemulsion was poured into a 250ml four-necked glass reactor equipped with a condenser and mechanical stirrer in a water bath. The stirring rate was kept at 300 rpm and polymerization was carried out for 1.5hr at 85℃

Conversion

The conversion of monomer was determined by gravimetric method. During miniemulsion polymerization, certain amount of the latex was taken out of the reactor, and poured into a hydroquinone methanol solution in an ice bath. Finally, the sample was dried in an oven at 85℃ until the weight kept constant. The conversion could be calculated by eq(1). P was the weight of dry sample from the oven. F was the theoretical weight of Fe_3O_4 in the sample. W was the weight of the latex sample and M_0 was the weight fraction of monomer in feed recipes.

$$Conversion = \frac{P - F}{W \times M_0} \times 100\% \quad (1)$$

Morphology of Oil-Based Fe_3O_4 and PS/Fe_3O_4 Composite Particles

The PS/Fe_3O_4 composite latex was diluted with deionized water and oil based Fe_3O_4 particles were dispersed in toluene. Then the sample was dropped on the surface of cooper grids, the morphology and particles size could be observed by using JOEL JEM-1230 transmission electron microscope (TEM)

Size Distributions of Monomer Droplets and Composite Latex Particles

The size distributions of the monomer droplets and composite latex particles were measured by laser dynamic light scattering instrument (Malvern Zeta Sizer 3000H). The sample was diluted with saturated styrene and SDS solution in order to avoid monomer or SDS diffuse from droplets to aqueous solution. The measurement could be completed within several minutes, and the size distribution was obtained and plotted by taking particle diameter as horizontal axis, cumulative volume percentage as vertical axis.

RESULTS AND DISCUSSION

Oil-Based Fe_3O_4 Particles

Figure 1 showed the XRD pattern of the oil-based Fe_3O_4 particles. The characteristic peaks were quite identical to pure Fe_3O_4[25], but the peaks were broader due to the nano size effect of Fe_3O_4 particles. The mean diameter of particles was calculated from the XRD pattern by Debye-Scherrer equation (shown in eq (2))[26,27]. D

was the average diameter of the crystal, λ was the wavelength of X-ray (CuKα=1.54Å), β was the width of the characteristic peak at half height and θ was the diffraction angle. The values of β and θ from peak (3 1 1) were used in eq(2) and the size of Fe_3O_4 crystal was calculated as 7.1nm.

$$D = \frac{0.9\lambda}{\beta \cos\theta} \quad (2)$$

The value of D was close to the diameter observed from TEM (Figure 2). However, the particles diameter from TEM ranged from 6nm to 9nm

PS/Fe_3O_4 Composite Particles

Effect of the Content of Fe_3O_4

Conversion curves of the obtained composite particles with different amount of Fe_3O_4 were shown in Figure 3. With increasing the content of the Fe_3O_4, the polymerization rate and final conversion decreased. That was because Fe^{2+} ions from Fe_3O_4 acted as a free radical quencher to inhibit the polymerization[17,28]. As a result, more Fe_3O_4 participated in the polymerization resulted in less effective free radicals and polymerization rate and final conversion would be suppressed. Figure 4 shows the size distributions of the initial droplets and final latex particles with different Fe_3O_4 contents. Fe-2, with 20% Fe_3O_4, whose droplet size distribution was broad and ranged from 300nm to 600nm. For Fe-1, with 10% Fe_3O_4, droplet size distribution shifted to smaller values, 200nm to 500nm, and for Fe_3O_4 free recipes, Fe-0, 50% of the droplets had diameter less than 200nm. It revealed that Fe_3O_4 dispersed in monomer would reduce the efficiency of droplets fission during ultrasonication and resulted in broader size distribution and larger average diameter of droplets.

After polymerization, Fe-1 and Fe-2 both had bimodal particle size distribution. The part of larger size particles mainly formed from the shrinking of original droplets and the part of smaller size particles mainly came from secondary nucleation. For Fe-0, unimodal particle size distribution was obtained because comparative amount of particles from both droplet shrinking and secondary nucleation resulted in a continuous distribution. Nevertheless, from the comparison of droplet and latex particle size distributions in these three experimental conditions, large population of composite particles formed from secondary nucleation.

TEM photographs of the obtained composite particles were shown in Figure 5. The results were consistent with the particle size distribution curves from dynamic light scattering experiment. With higher content of Fe_3O_4, the size of larger composite particles increased. The reason was that larger original droplets resulted in larger composite particles even after shrinking. However changing the Fe_3O_4 content would not change the morphology of composite particles and the distribution of Fe_3O_4 in PS latex particles was random and quite homogenous.

Effect of the Homogenized Energy

The homogenization energy applied to the O/W emulsion could be varied by adjusting the ultrasonication time and amplitude, the longer ultrasonication time and higher ultrasonication amplitude reflected more energy. In Figure 6, the conversion curves of the composite latex showed that increasing the ultrosinication energy, the polymerization rate would be promoted. It appeared that more energy applied to the O/W emulsion, the monomer would split into more small droplets. In other words, during polymerization, the reaction site for droplet nucleation increased and the polymerization rate would be enhanced.

The explanation could be verified by Figure 7, when homogenization energy applied from Energy-1 to Energy-3, the droplet distribution would become narrower and the average particle size shifted to a smaller value. Furthermore, after polymerization, Energy-3 had similar size distribution curve between droplets and composite particles. It implied that the possibility of secondary nucleation was largely reduced. In other words, most particles formed from droplet nucleation. However, for Energy-1 and Energy-2, significantly shrinking feature was observed due to the fact that the critically stabilized size of droplets was not achieved before polymerization. Therefore, the secondary nucleation dominated over the droplet nucleation especially in the system of Energy-1. It could be concluded that homogenization energy played an important role to control the nucleation mechanism and enough energy was required to attain droplet nucleation.

TEM photographs of the synthesized composite particles were shown in Figure 5(b) for Energy-1 and in Figure 8 for Energy-3. The results showed that the morphology of composite particles

would change from homogeneous to core-shell with Fe_3O_4 on the shell. As increasing the homogenization energy during ultrasonication, Fe_3O_4 particles were forced out from the monomer droplets to the surfaces due to the large density difference between Fe_3O_4 and styrene.

Effect of Surfactant Concentration

The function of surfactant, SDS, was to keep the droplets from coalescence and provide enough electrostatic repulsive force to maintain the stability of monomer droplets. The conversion curves with different surfactant concentrations were shown in Figure 9 and the polymerization rate was in the order of SDS-3> SDS-2> SDS-1. It could be explained by Figure 10, where the size of monomer droplets was in the order of SDS-3< SDS-2< SDS-1. When the amount of surfactant increased, more surfactant could stabilize the O/W surfaces. Monomer would split into smaller and more droplets during the process of ultrasonication. Since small monomer droplets acted as reaction loci, the polymerization rate was increased with increasing the number of droplets and the average size of composite particles decreased.

After polymerization, the shrinking phenomenon of particles in comparison with the size of initial droplets was obvious in SDS-1 and SDS-3 than SDS-2, the resulting average diameter of composite particles was smaller than their corresponding initial droplets. This result indicated that SDS-2 was an optimum concentration among three for surfactant in miniemulsion polymerization. For SDS-1, insufficient amount of surfactant could not provide enough stabilization for O/W surfaces, thus enhanced the possibility of secondary nucleation. As for SDS-3, superfluous surfactant would form micelles and monomer could diffuse from droplets into micelles and induced micellar nucleation. In our study, 35mM was an adequate concentration of surfactant SDS to achieve droplet nucleation. In SDS-2, size distributions of the droplets and composite particles were similar, indicating the fact that droplet nucleation dominated.

Furthermore, compared the TEM photographs of SDS-1 and SDS-2 (shown in Figure 11 and Figure 8), less Fe_3O_4 containing latex particles were observed for SDS-1, It was due to that, insufficient amount of surfactant could not provide enough protection for Fe_3O_4 particles dispersing in styrene and phase separation occurred during ultrasonication.

Effect of the Costabilizer

The role of costabilizer was to suppress Oswald ripening effect by introducing osmotic pressure and maintain the droplet stability under polymerization. In this series of experiment, HD and Span 20 were chosen as two types of costabilizer where HD was a highly hydrophobic compound and Span 20 was relatively more hydrophilic due to its shorter hydrocarbon chain and having three hydrophilic hydroxyl functional groups. Their structures were shown in Scheme 1. Due to the amphiphilic nature of Span 20, it could also be used as a surfactant (HLB=8.6). Compared the conversion curves of HD-1, Span -1 and HD-2, Span-2 in Figure 12. Regardless the homogenization energy was high or low, when the costabilizer changed from HD to Span 20, the polymerization rate was accelerated. It was because that Span 20 acted not only as a costabilizer but also as a surfactant, more surfactant was available to stabilize the O/W surfaces during ultrasonication. Thus the number of monomer droplets, which could be as the reaction site, increased. The result could be verified by the size distribution curves of HD-2 and Span-2 in Figure 13, the size of droplet of HD-2 was larger than that of Span -2 as expected.

Compared the size distributions of droplets and latex particles for HD-2 and Span-2, it was found that, Span-2 had at least 30% monomer droplets with same distribution as latex particles, while at least 50% for HD-2. The result showed that hydrophobic costabilizer increased the possibility of droplet nucleation.

The morphology difference with different costabilizer could be observed by TEM photographs in Figure 5(b) and Figure 14(a). Compared these two photographs, the morphology of composite particles changed from homogeneous for HD-1 to core-shell with Fe_3O_4 on the shell for Span-1. This was resulted from the more hydrophilic structure of Span 20, which could bring Fe_3O_4 particles out onto the surfaces from the monomer droplets during ultrasonication or early stage of polymerization, whereas Fe_3O_4 particles still distributed homogeneously in styrene droplets when using HD as a costabilizer. The morphology of HD-2 and Span-2 (showed in Figure 8 and Figure 14(b)) was all in core-shell, the homogeneous morphology was not observed. It was due to that high homogenization energy applied determined the morphology of composite particles.

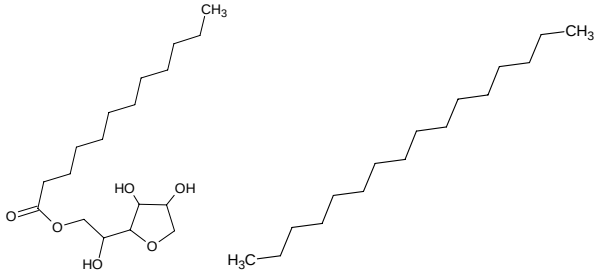

Span 20 HD

Scheme 1.chemical structures of Span 20 and HD

CONCLUSION

In this work, PS/Fe_3O_4 composite particles were synthesized successfully from miniemulsion polymerization. The conversion curves, size distributions of droplets and latex particles, nucleation mechanism and morphology were discussed in detail. Polymerization rate could be promoted by increasing the number of monomer droplets, which could be achieved under the condition of high concentration of surfactant, higher homogenization energy or changing costabilizer form HD to Span 20. Because of the role of Fe^{2+} from Fe_3O_4 acted as a free radical quencher, more Fe_3O_4 participated in the reaction would reduce the polymerization rate.

The size distributions of droplets and latex particles were measured and compared to estimate the fraction of droplet nucleation. With increasing the Fe_3O_4 content, the size distribution of droplets and latex particles were broader with more population of larger particles due to the less efficiency of droplet fission during ultrasonication. For high homogenization energy recipe, the monomer droplets were critically stabilized, the size distributions of monomer droplet and its resulting latex particles were almost identical. The function of SDS was to provide stabilization for O/W surfaces, an optimum concentration was found. Too much surfactant would generate micelles and induced micellar nucleation. Insufficient amount of surfactant could not maintain the stability of monomer droplets and secondary nucleation could not be avoided. The choice of costabilizer was critical too, more hydrophobic one, HD, was effective to produce osmotic pressure and resist Oswald ripening effect. Thus, the stability of monomer droplet was enhanced and polymerization in situ, droplet nucleation dominated.

Morphology of composite latex particles could be well controlled via changing homogenization energy and costabilizer. For high homogenization energy recipe, the Fe_3O_4 located on the surface of PS latex particles. It differed from the one with low homogenization energy, where Fe_3O_4 was random and quite homogeneously distributed inside the latex particles. It was due to that more possibility for Fe_3O_4 particles to be ultrasonicated out from the interior of monomer droplets to surfaces under high homogenization energy. When HD was used as a costabilizer, random and quite homogeneous morphology could be observed for composite particles if homogenization energy was not high. However, the core-shell morphology with Fe_3O_4 on the shell of composite particles was observed if Span 20 replaced HD as a costabilizer. The more hydrophilic nature of Span 20 changed the location of Fe_3O_4 particles and induced the morphology change. The morphology control could afford different applications of these magnetic composite particles.

REFERENCE

1. Haik, Y.;Pai V.; Che, C.J.J Magn Magn Mater 1999,194,254.
2. Seiben, S.; Bergemann, C.; Lubbe, A.; Brockmann, B.; Rescheleit, D.J Magn Magn Mater 2001, 225, 175.
3. Akgol, S.; Yasemin, K.; Denizli, A.; Arica, M. Y. Food Chem 2001, 74, 281.
4. Pyle, B. H.; Broadaway, S. C.; McFeters, G. A. Appl Environ Microbiol 1999, 65, 1966.
5. Cheng, F. Y.; Su, C. H.; Yang, Y. S.; Yeh, C. S.;Tsai, C. Y.;Wu, C. L.;Wu, M. T.; Shieh, D. B. Biomaterials 2005, 26, 729.
6. Viroonchatapan, E.; Ueno, M.; Sato, H.; Adachi, I.; Nagae, H.; Tazawa, K.; Horikoshi, I. Pharm Res 1995, 12, 1176.
7. Gupta, P.K.; Hung, C.T. Life Sci. 1989, 44, 175.
8. Yanase, N.; Noguchi, H.; Asakura, H.; Suzuta, T. J Appl Polym Sci 1993, 50, 765.
9. Deng, Y.H.; Yang, W.L.; Wang, C.C.; Fu, S.K. AdvMater 2003, 15, 1729.
10. Pollert, E.; Knizek, K.; Marysko, M.; Zaveta, K.; Lancok, A.; Bohacek, J.; Horak, D.; Babic, M. Journal of Magnetism and Magnetic Materials 2006**,** 306, 241.
11. Wang, P. C.; Chiu, W. Y.; Lee, C. F.;Young, T. H.; J Polym Sci Part A:Polym Chem 2005,43,1343.
12. Pich, A.; Bhattacharya, S.; Ghosh, A.; Adler, H. J. P. Polymer 2005**,** 46, 4596.
13. Csetneki, I.; Faix, M. K.; Szilagyi, A.; Kovacs, A. L.; Nemeth,

Z.; Zrinyi, M. J Polym Sci Part A:Polym Chem 2004, 42, 4802.

14. Wormuth, K. J Colloid Interface Sci 2001**,** 241, 366.
15. Lu, S. H.; Forcada, J. J Polym Sci Part A:Polym Chem 2006, 44, 4187.
16. Ramirez, L. P.; Landfester, K. Macromol Chem Phys 2003, 204, 22.
17. Lin, C.L.; Chiu, W.Y.; Don, T.M. J Polym Sci Part A:Polym Chem 2006, 100, 3987.
18. Deng, Y.; Wang, L.; Yang, W.; Fu, S.; Elaıssari, A. J Magn Magn Mater 2003, 257, 69.
19. Kataby, G.; Cojocaru, M.; Prozorov, R.; Gedanken, A. Langmuir 1999**,** 15, 1703.
20. Erdem, B.; Sudol, ED.; Dimonie, VL.; EL-Aasser, MS. Macromol. Symp. 2000, 155, 181.
21. Petre, M.;Costa, L.C.; Neves, A.; Soares, M.J.; Monteiro, T.; Esteves, A.C.; Barros-Timmons, A.; Trindade, T.; Kholkin, A.; Alves, E. Nanotechnology 2005, 16, 1969.
22. Tiarks, F.; Landfester, K.; Anonietti, M. Macromol. Chem. Phys. 2001, 202, 51.
23. Zhang, J.; Gao,G.; Zhang,M.; Zhang,D.; Wang,Cl; Zhao,D.; Liu,F. J Polym Sci Part A:Polym Chem 2006, 301, 78.
24. Bechthold, N.; Tiarks, F.; Willert, M.; Landfester, K.; Antinietti, M. Macromol Symp 2000, 151, 549.
25. Schwertmann, U.; Cornell, M.R. Iron Oxides in the Laboratory, Preparation and Characterization, VCH, New York, 1991.
26. Massart, R.; Cabuil, V. J. Chim. Phys. Phys. Chim. Biol. 84, 1987, 967.
27. A. Taylor, X-Ray Metallography, Wiley, New York, 1961, 674.
28. Bataille, P.; Van, B. T.; Pham, Q. B. J Polym Sci Polym Chem Ed 1982, 20, 811.

Table 1. Symbols and Recipes for Synthesized Composite Particles

	Fe_3O_4 (%)	SDS (mM)	Costabilizer	Energy	AIBN (wt%)
Fe-0	0	35	HD	50%,13min	2.5
Fe-0.5	5	35	HD	50%,13min	2.5
Fe-1	10	35	HD	50%,13min	2.5
Fe-2	20	35	HD	50%,13min	2.5
Energy-1	10	35	HD	50%,13min	2.5
Energy-2	10	35	HD	50%,30min	2.5
Energy-3	10	35	HD	100%,30min	2.5
SDS-1	10	20	HD	100%,30min	2.5
SDS-2	10	35	HD	100%,30min	2.5
SDS-3	10	70	HD	100%,30min	2.5
HD-1	10	35	HD	50%,13min	2.5
Span-1	10	35	Span 20	50%,13min	2.5
HD-2	10	35	HD	100%,30min	2.5
Span-2	10	35	Span 20	100%,30min	2.5

Styrene + Fe_3O_4 =13.89g , Costabilizer concentration=51mM

The percentage of initiator was based on monomer

The percentage of Fe_3O_4 was based on styrene + Fe_3O_4

The concentration of surfactant or costabilizer was based on water

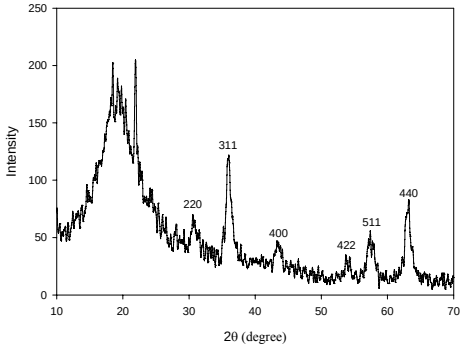

Figure 1. XRD pattern of oil-base Fe_3O_4

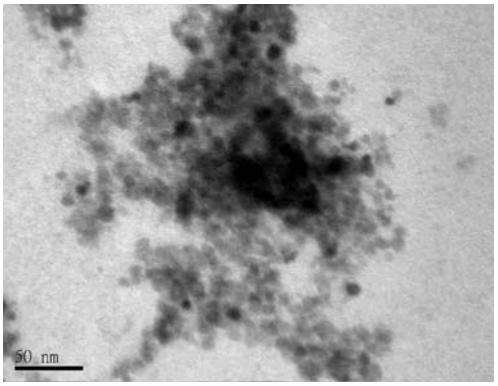

Figure 2. TEM photograph of oil-base Fe_3O_4 particles

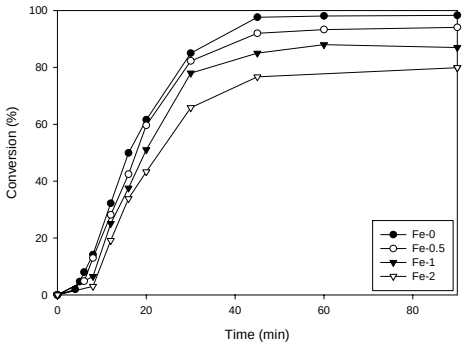

Figure 3. Monomer conversion versus time with different amount of Fe_3O_4

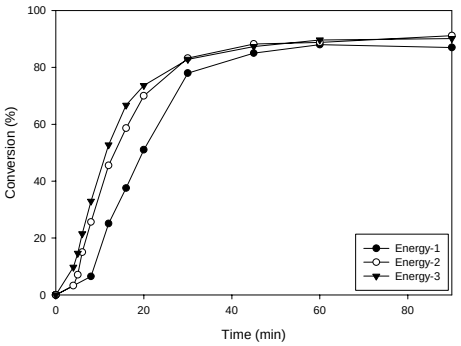

Figure 6. Monomer conversion versus time with different homogenized energy

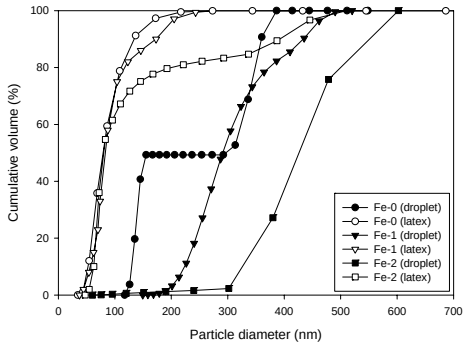

Figure 4. Size distributions of droplets and latex particles with different amount of Fe_3O_4

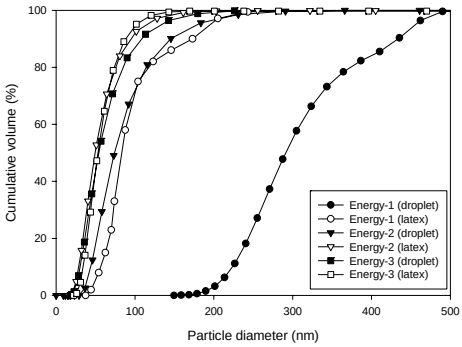

Figure 7. Size distributions of droplets and latex particles with different homogenized energy

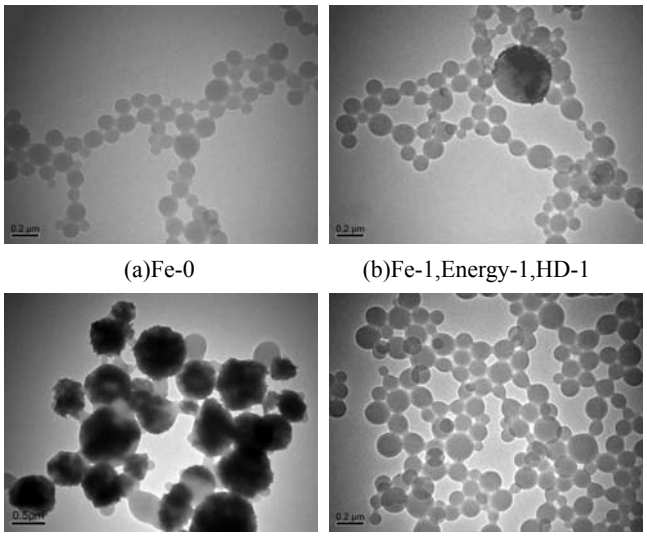

(a)Fe-0 (b)Fe-1,Energy-1,HD-1

(c)Fe-2

Figure 5. TEM photographs of synthesized composite latex particles with different amount of Fe_3O_4

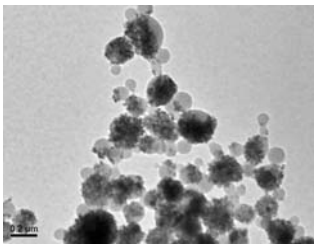

Figure 8. TEM photographs of synthesized composite particles Energy-3, SDS-2, HD-2.

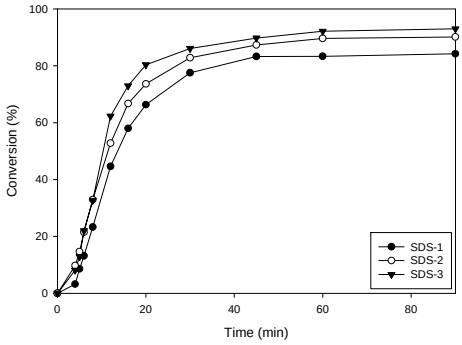

Figure 9. Monomer conversion versus time with different amount of SDS

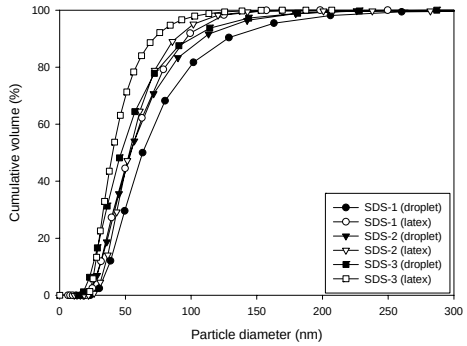

Figure 10. Size distributions of droplets and latex particles with different amount of SDS

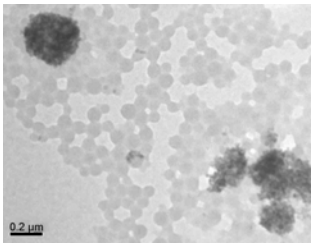

Figure 11. TEM photographs of synthesized composite particles SDS-1

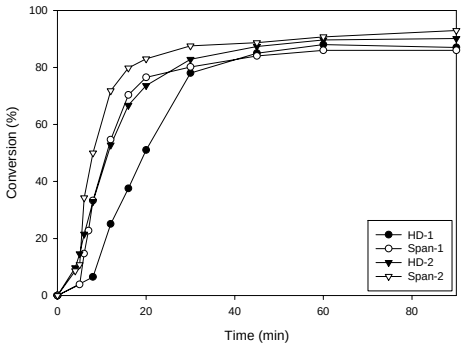

Figure 12. Monomer conversion versus time with different costabilizer

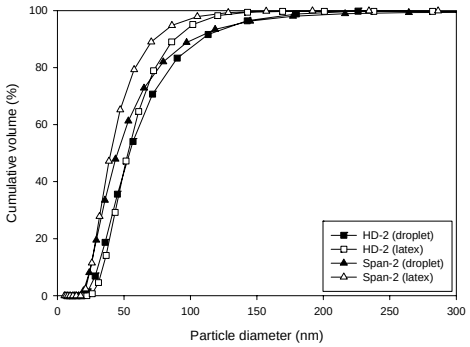

Figure 13. Size distributions of droplets and latex particles with different costabilizer

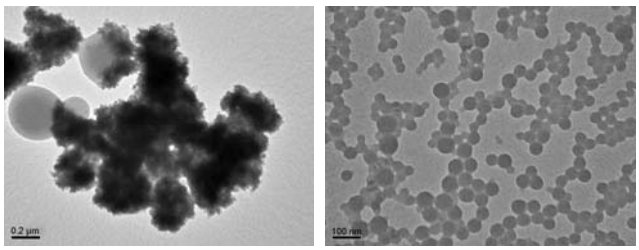

(a)Span-1

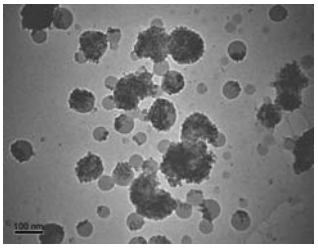

(b)Span-2

Figure 14. TEM photographs of synthesized composite particles

PARTⅣ：Morphology of PU/PMMA Hybrid Particles from Miniemulsion Polymerization: Thermodynamic Considerations

ABSTRACT: The morphology of PU/PMMA hybrid particles prepared by miniemulsion polymerization was predicted through the consideration of their Gibbs free energy changes. Five morphological states of PU/PMMA hybrid particles were proposed and their Gibbs free energy changes were calculated. Before the formation of hybrid particles,the initial state included a monomer mixture of PU prepolymer, MMA, a chain extender, TMP, and an initiator, which was in droplets suspended in water containing SDS. Two assumptions were made. First, the densities of all states were the same. Secondly, secondary nucleation of particles was negligible. Thus the size of initial droplet and final particle was unchanged through miniemulsion polymerization. The interfacial tensions were measured by a pendant drop method and were used for calculation. The preferred morphology of PU/PMMA hybrid particle had the minimum value of ΔG_{phase}. Different NCO/OH ratios of PU and initiators of MMA were used to study the morphological change of PU/PMMA hybrid particles. When BD was used as the chain extender of PU, the hybrid particles showed the PU-rich phase as the shell and PMMA-rich as the core. When incorporating bisphenol A into PU polymer, the homogeneous structure of hybrid particle was preferred.

Keywords: morphology; polyurethanes; thermodynamics

INTRODUCTION

To achieve better mechanical properties and higher colloid stability, a hybrid polymer particle containing two polymers is generally prepared as designed.[1–3] In recent years, miniemulsion polymerization is a new way to prepare the hybrid particle. There are some documents of preparing core-shell latex through miniemulsion polymerization.[4–7] However, the morphological changes of the hybrid particles with experimental variables, such as compositions of monomers, types of initiators, and other polymerization conditions, were not fully understood.

Most polymer blends contain thermodynamically immiscible components. Their morphology usually has a larger influence on mechanical properties. It is well known that the morphology of polymer blends is influenced by the blend composition, preparation conditions, and interfacial tension between two polymers. Latex system with well-designed particle morphology is useful to manufacture advanced engineering plastics with high tensile strength, improved toughness, and other high-added values. Composite latex particles of different morphologies are usually prepared by seeded emulsion polymerization techniques where a second monomer is synthesized in the presence of seed latex particles. Investigation of the morphology of core-shell latex and the factors controlling it are the goal of many papers published in previous years. Most researched systems in the literatures are PS/PMMA[8–10] and PS/PBA.[11,12] In these earlier documents, the controlling factors fall into two broad categories: thermodynamics and kinetics. Thermodynamic factors determine the equilibrium morphology of final particles, whereas kinetic ones determine the ease of such thermodynamically favored morphology.

In the aspects of thermodynamics, Torza and Mason[13] first showed the interfacial behavior of systems including three immiscible liquids. They examined the required states for a liquid to engulf an initial droplet when both were immersed in a continuous phase. Their analysis showed that the interfacial tension was one of the main factors controlling the morphology of particles. Dimonie et al.[14] also reported the viscosity of the polymerization locus, which related to the chain mobility influenced morphology as well. The following work from Chen et al.[15] demonstrated an important mathematical model combining the study of Sundberg et al.[16] to describe the free energy changes corresponding to PS/PMMA latex morphology. This model combining the analysis of interfacial tension predicted the latex morphology successfully.

In addition, methods to measure interfacial tension between immiscible fluid phases have been developed for many years. For instance, Van der Waals acid–base approach,[17] the soap titration,[11] drop-weight volume,[18] and pendant drop[19–21] could be used to determine interfacial tensions. Other methods have been reviewed in detail by Rusanov and Prokhorov.[22] In our work, the pendant drop was used to measure the interfacial tension. This method has the following advantages: it is a simple-mathematical analysis; results are independent of the contact angle between the fluid interface and the apparatus; photographs of drop-shape can be analyzed instantaneously; it is a static method and therefore

would not be influenced by viscosity; only small samples are needed and high accuracy results can be obtained.

By thermodynamic consideration, the Gibbs free energy changes of PU/PMMA hybrid particles prepared from miniemulsion polymerization were calculated and related to the morphology.

THERMODYNAMIC CONSIDERATIONS OF THE PARTICLE MORPHOLOGY

By considering the following assumptions for morphology development in miniemulsion polymerization, the change of Gibbs free energy was regarded as the driving force. As shown in Figure 1, the initial state included a monomer mixture of PU prepolymer, MMA, a chain extender, TMP, and an initiator, which was in droplets suspended in water containing SDS. Five possible states of final particles were considered in this study. The total Gibbs free energy change can be expressed as

$$\Delta G_{\text{total}} = \Delta G_{\text{poly}} + \Delta G_{\text{phase}}$$

ΔG_{poly}: from the polymerization; ΔG_{phase} from the change of morphology and interfacial tension.

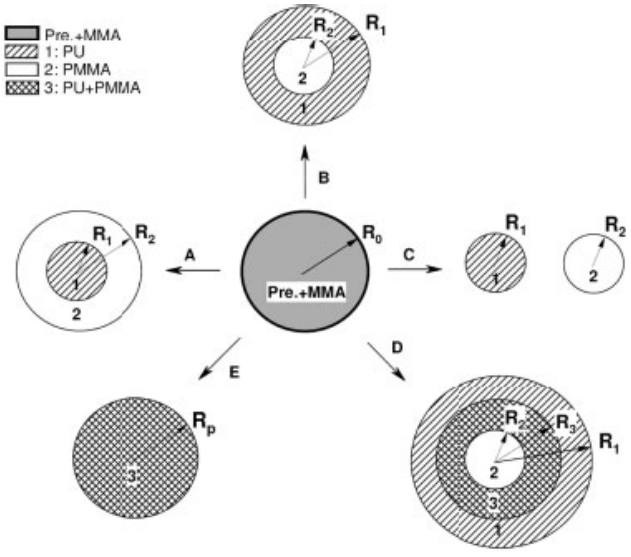

Figure 1. Morphological states of PU/PMMA hybrid particles.

Because polymerization occurred, $\Delta G_{poly} < 0$. If the final state could be formed, ΔG_{total} should be negative. Hence, the value of ΔG_{phase} would determine the morphology of the final state. In this work, we thus focused on the Gibbs free energy change (ΔG_{phase}) from the change of morphology and interfacial tension.

Equations for ΔG_{phase}

From thermodynamic equation, the internal energy U at constant temperature is

$dU = T\,dS + dW$

where T is temperature, S is entropy, and W is work done by the system.

The change of morphology of particles from initial to final state creates new interfaces. If the surface tension γ is a real force acting along the surface, it will produce the work γdA, where A is the surface area. Then we get

$$dW = \gamma\, dA - d(PV)$$

$$dU = T\, dS + \gamma\, dA - d(PV)$$

The integrating form at constant pressure is

$$U = TS + \gamma A - PV$$

Hence, the Gibbs free energy is

$$\begin{aligned} G_{\text{phase}} &= H - TS \\ &= U + PV - TS \\ &= \gamma A \end{aligned}$$

And the total Gibbs free energy change can Be expressed as

$$\Delta G_{\text{phase}} = \Delta(\gamma A)$$

Or

$$\Delta G_{\text{phase}} = \sum \gamma_{ij} A_{ij} - \gamma_{\text{mw}} A_{\text{mw}} \qquad (1)$$

where γ_{ij} is the interfacial tension between i and j and A_{ij} is the corresponding interfacial area. γ_{mw} is the interfacial tension of initial monomer droplet suspended in water and A_{mw} is its interfacial area. Each of the final states, A–E in Figure 1, had different total Gibbs free energy change due to its different morphology.The thermodynamically preferred morphology of a system will be the one that had minimum value of ΔG_{phase}. If all γ_{ij} can be measured, the Gibbs free energy change can be calculated. Thus, the prediction of preferred morphology resulted in a practical application. Two important assumptions were made as: (1) the densities of all states were the same; (2) secondary

nucleation of particles was negligible. Thus the size of initial droplet and final particle was unchanged through miniemulsion polymerization. Following was the description of Gibbs free energy change per unit area for five final states.

State A: PU as the Core and PMMA as the Shell

The Gibbs free energy change for state A was

$$\begin{aligned}\Delta G_{\mathrm{a}} &= \gamma_{12}A_{12} + \gamma_{2\mathrm{w}}A_{2\mathrm{w}} - \gamma_{\mathrm{mw}}A_{\mathrm{mw}} \\ &= \gamma_{12}4\pi R_1^2 + \gamma_{2\mathrm{w}}4\pi R_2^2 - \gamma_{\mathrm{mw}}4\pi R_0^2 \end{aligned} \quad (2)$$

where γ_{12}, $\gamma_{2\mathrm{w}}$, and γ_{mw} were the interfacial tensions between the phases of PU/PMMA, PMMA/water and monomers/water, respectively. R_1, R_2, and R_0 were the radius of PU core, final particle, and initial droplet, respectively. To describe the free energy change per unit surface area of initial droplet, eq 2 could be rearranged as

$$\Delta\psi_{\mathrm{a}} = \frac{\Delta G_{\mathrm{a}}}{4\pi R_0^2} = \gamma_{12}\left(\frac{R_1}{R_0}\right)^2 + \gamma_{2\mathrm{w}}\left(\frac{R_2}{R_0}\right)^2 - \gamma_{\mathrm{mw}} \quad (3)$$

where $\Delta\Psi_{\mathrm{a}}$ was the free energy change per unit area of particle.

To define the volume fraction of PMMA in the final particle, ϕ_2 as

$$\begin{aligned}\phi_2 &= \frac{V_2}{V_t} = \frac{\frac{4}{3}\pi R_2^3 - \frac{4}{3}\pi R_1^3}{\frac{4}{3}\pi R_2^3} = \frac{R_2^3 - R_1^3}{R_2^3} = 1 - \left(\frac{R_1}{R_2}\right)^3 \\ &\Rightarrow \frac{R_1}{R_2} = (1-\phi_2)^{1/3} \end{aligned} \quad (4)$$

By Using R_2=R_0 (for ideal miniemulsion) and ϕ_2, eq 3 turned into

$$\Delta\psi_{\mathrm{a}} = \gamma_{12}(1-\phi_2)^{2/3} + \gamma_{2\mathrm{w}} - \gamma_{\mathrm{mw}} \quad (5)$$

State B: PMMA as the Core and PU as the Shell

Similar analysis was applied to state B as follows:

$$\begin{aligned}\phi_2 &= \frac{V_2}{V_t} = \frac{\frac{4}{3}\pi R_2^3}{\frac{4}{3}\pi R_1^3} = \frac{R_2^3}{R_1^3} = \left(\frac{R_2}{R_1}\right)^3 \\ &\Rightarrow \frac{R_2}{R_1} = \phi_2^{1/3} = \frac{R_2}{R_0} \end{aligned}$$

$$\begin{aligned}\Delta G_{\mathrm{b}} &= \gamma_{12}A_{12} + \gamma_{1\mathrm{w}}A_{1\mathrm{w}} - \gamma_{\mathrm{mw}}A_{\mathrm{mw}} \\ &= \gamma_{12}4\pi R_2^2 + \gamma_{1\mathrm{w}}4\pi R_1^2 - \gamma_{\mathrm{mw}}4\pi R_0^2 \end{aligned}$$

and

$$\begin{aligned}\Delta\psi_{\mathrm{b}} = \frac{\Delta G_{\mathrm{b}}}{4\pi R_0^2} &= \gamma_{12}\left(\frac{R_2}{R_0}\right)^2 + \gamma_{1\mathrm{w}}\left(\frac{R_1}{R_0}\right)^2 - \gamma_{\mathrm{mw}} \\ &= \gamma_{12}\phi_2^{2/3} + \gamma_{1\mathrm{w}} - \gamma_{\mathrm{mw}} \end{aligned} \quad (6)$$

State C: Individual Particles of PMMA and PU

The volume fraction of PMMA was as

$$\begin{aligned}\phi_2 &= \frac{V_2}{V_t} = \frac{\frac{4}{3}\pi R_2^3}{\frac{4}{3}\pi R_1^3 + \frac{4}{3}\pi R_2^3} = \frac{R_2^3}{R_1^3 + R_2^3} = \frac{1}{\left(\frac{R_1}{R_2}\right)^3 + 1} \\ &\Rightarrow \frac{R_1}{R_2} = \left(\frac{1}{\phi_2} - 1\right)^{1/3} \end{aligned}$$

Here R_0=R_1=R_2, therefore

$$\begin{aligned}\phi_2 &= \frac{V_2}{V_t} = \frac{R_2^3}{R_0^3} \\ &\Rightarrow \frac{R_2}{R_0} = \phi_2^{1/3} \\ &\Rightarrow \frac{R_1}{R_0} = (1-\phi_2)^{1/3} \end{aligned}$$

The free energy change was expressed as

$$\begin{aligned}\Delta G_{\mathrm{c}} &= \gamma_{1\mathrm{w}}A_{1\mathrm{w}} + \gamma_{2\mathrm{w}}A_{2\mathrm{w}} - \gamma_{\mathrm{mw}}A_{\mathrm{mw}} \\ &= \gamma_{1\mathrm{w}}4\pi R_1^2 + \gamma_{2\mathrm{w}}4\pi R_2^2 - \gamma_{\mathrm{mw}}4\pi R_0^2 \end{aligned}$$

and

$$\begin{aligned}\Delta\psi_{\mathrm{c}} = \frac{\Delta G_{\mathrm{c}}}{4\pi R_0^2} &= \gamma_{1\mathrm{w}}\left(\frac{R_1}{R_0}\right)^2 + \gamma_{2\mathrm{w}}\left(\frac{R_2}{R_0}\right)^2 - \gamma_{\mathrm{mw}} \\ &= \gamma_{1\mathrm{w}}(1-\phi_2)^{2/3} + \gamma_{2\mathrm{w}}\phi_2^{2/3} - \gamma_{\mathrm{mw}} \end{aligned} \quad (7)$$

State D: PMMA as the Core, PU/PMMA as the Intermediate Layer, and PU as the Shell

First, we defined the weight fraction of PU (x) and volume fraction of PMMA (ϕ2). Thus the relation of R_1, R_2, and R_3 was as

$$x = \frac{W_{PU}}{W_{PU} + W_{PMMA}}$$

$$\phi_2 = \frac{V_2}{V_t} = 1 - x$$
$$=> \frac{R_2^3 + \phi_{32}(R_3^3 - R_2^3)}{R_1^3} = 1 - x$$
$$=> \phi_{32}\left(\frac{R_3}{R_1}\right)^3 + \phi_{31}\left(\frac{R_2}{R_1}\right)^3 = 1 - x$$
$$=> \left(\frac{R_3}{R_1}\right)^3 = \frac{1-x}{\phi_{32}} - \frac{\phi_{31}}{\phi_{32}}\left(\frac{R_2}{R_1}\right)^3 \text{ or}$$
$$\left(\frac{R_2}{R_1}\right)^3 = \frac{1-x}{\phi_{31}} - \frac{\phi_{31}}{\phi_{31}}\left(\frac{R_3}{R_1}\right)^3$$

where ϕ_{31} and ϕ_{32} are the volume fractions of PU and PMMA in the intermediate layer, respectively.

As a result, the free energy change can be expressed in terms of R_2/R_0

$$\Delta G_d = \gamma_{23}A_{23} + \gamma_{13}A_{13} + \gamma_{1w}A_{1w} - \gamma_{mw}A_{mw}$$
$$= \gamma_{23}4\pi R_2^2 + \gamma_{13}4\pi R_3^2 + \gamma_{1w}4\pi R_1^2 - \gamma_{mw}4\pi R_0^2$$

and

$$\Delta\psi_d = \frac{\Delta G_d}{4\pi R_0^2} = \gamma_{23}\left(\frac{R_2}{R_0}\right)^2 + \gamma_{13}\left(\frac{R_3}{R_0}\right)^2 + \gamma_{1w}\left(\frac{R_1}{R_0}\right)^2 - \gamma_{mw}$$
$$= \gamma_{23}\left(\frac{R_2}{R_0}\right)^2 + \gamma_{13}\left(\frac{\phi_2}{\phi_{32}} - \frac{\phi_{31}}{\phi_{32}}\left(\frac{R_2}{R_0}\right)^3\right)^{2/3}$$
$$+ \gamma_{1w} - \gamma_{mw} \quad (8)$$

State E: Homogeneous PU/PMMA Particle

If there was no phase separation occurred through miniemulsion polymerization, the free energy change was expressed as

$$\Delta G_e = \gamma_{pw}A_{pw} - \gamma_{mw}A_{mw} = \gamma_{pw}4\pi R_p^2 - \gamma_{mw}4\pi R_0^2$$
$$\Delta\psi_e = \frac{\Delta G}{4\pi R_0^2} = \gamma_{pw}\left(\frac{R_p}{R_0}\right)^2 - \gamma_{mw} = \gamma_{pw} - \gamma_{mw} \quad (9)$$

Therefore, by measuring the interfacial tension, the free energy change could be calculated from eqs 5–9 for five final states of particles, respectively.

EXPERIMENTAL

Materials

Isophorone diisocyanates (IPDI; Lancaster), 1,4-butanediol (BD; TEDIA), bisphenol A (BisA; TCI), trimethylol propane (TMP; ACROS), dibutyltin dilaurate (SnDBL; TCI), sodium dodecyl sulfate (SDS; TCI), hexadecane (HD; TCI), benzoyl peroxide (BPO; ACROS), potassium persulfate(KPS; TCI), and hydroquinone (HQ; TCI) were used without further purification. Polypropylene glycol (PPG; Showa), with an average molecular weight of 1000 (g/mol), was dried under vacuum at 80 8C for 24 h before use. Methyl methacrylate (MMA; Showa) was distilled to remove impurities and then stored in refrigerator before use.

Synthesis of PU Prepolymer The synthesis of PU prepolymer was carried out in a 100-mL round-bottom, three-necked flask with a magnetic stirrer, thermometer, condenser, nitrogen inlet, and an outlet. Reaction temperature was set at 60 8C and was controlled by immersion in an isothermal oil bath. IPDI (1.23 g) and PPG1000 (2.76 g) dissolved in MMA (1.6 g) were charged into the flask and then heated to the reaction temperature. Subsequently, SnDBL catalyst (0.1 wt % based on the total monomer weight) was added into the solution. The equivalent ratio of IPDI and PPG1000 was 2/1. The theoretical NCO value was determined using a standard dibutylamine back titration method. After achieving the theoretical NCO value, NCO-terminated prepolymers were cooled down to room temperature and then were stored in refrigerator before use. Synthesis of PU Latex An oil phase, NCO-terminated prepolymers (5.59 g), isophorone diisocyanates (0.86 g; if needed), hexadecane (4.4 wt %), 1,4-butanediol (0.125 g) or bisphenol A (0.315 g), dibutyltin dilaurate (0.1 wt %), and trimethylol propane (0.125 g) were stirred together. Sodium dodecyl sulfate (0.8 wt %) was dissolved in deionized water as a water phase. Then the oil and water phases were mixed and stirred for 10 min. Preemulsion was prepared by ultrasonifying the mixtures for 12 min. All the above steps were proceeded in an ice bath to prevent the premature polycondensation reaction. The miniemulsion was introduced to a 250-mL round-bottom, four-necked separable flask with a mechanical stirrer, thermometer, condenser, nitrogen inlet, and an outlet. Synthesis of PU latex was carried out at 70 8C for 3 h. To obtain the dried PU latex, samples were washed with water, filtered, and dried by lyophilization. Two different chain extenders were used to obtain PU polymers. The first one was BD chain extender with NCO/OH 1.7, 1.0 (BD/1.7; BD/1.0) and the second one was BisA chain extender with NCO/OH 1.0 (BisA/1.0).

Synthesis of PMMA Latex

Two kinds of initiators were used: BPO and KPS. In an oil phase, MMA (16.13 g), HD (4.4 wt %), and initiator (1 wt %) were stirred together. SDS (0.8 wt %) was dissolved in deionized water as a water phase. Then the oil and water phases were mixed and stirred. A miniemulsion was prepared by ultrasonifying the mixtures for 12 min. All the above steps were proceeded in an ice bath. The miniemulsion was introduced to a 250-mL round-bottom, fournecked separable flask with a mechanical stirrer, thermometer, condenser, nitrogen inlet, and an outlet. After 5 min, KPS (if needed) was added into reactor. Synthesis of PMMA latex was carried out at 70 8C for 3 h. To obtain the dried PMMA latex, samples were washed with water, filtered, and dried by lyophilization. Two different PMMA were synthesized, namely, PMMA-BPO from BPO initiator and PMMA-KPS from KPS initiator.

Synthesis of PU/PMMA Hybrid Latex

In an oil phase, NCO-terminated prepolymer (5.59 g), MMA (15.37 g), HD (4.4 wt %), BD (0.125 g), SnDBL (0.1 wt %), TMP (0.125 g), and BPO (1 wt %) were stirred together. SDS (0.8 wt %) was dissolved in deionized water as a water phase. Then the oil and water phases were mixed and stirred. A miniemulsion was prepared by ultrasonifying the mixtures for 12 min. All the above steps were proceeded in an ice bath to prevent the premature polymerization reaction. The miniemulsion was introduced to a 250-mL round-bottom, four-necked separable flask with a mechanical stirrer, thermometer, condenser, nitrogen inlet, and an outlet. Synthesis of PU/PMMA polymer was carried out at 70 8C for 3 h.

Analysis

Contact Angle Measurements

PU and PMMA latex were poured into steel molds at 100℃ for 24 h and their films were obtained. Two liquids, water and ethylene glycol, were used as the probe liquids. A releasing probe liquid (0.05 mL) was dropped onto the surface of polymer film from a syringe. Contact angles of each drop (θ_w and θ_{EG}) were recorded by the instrument, Olympus, model SZ-ST. Three drops were taken to give the value in average. As shown in Table 1, there were five kinds of polymer films. Furthermore, from the transform Harmonic-mean equation,23

$$(1+\cos\theta_{\mathrm{w}})\gamma_{\mathrm{w}} = 4\left(\frac{\gamma_{\mathrm{w}}^{\mathrm{d}}\gamma^{\mathrm{d}}}{\gamma_{\mathrm{w}}^{\mathrm{d}}+\gamma^{\mathrm{d}}} + \frac{\gamma_{\mathrm{w}}^{\mathrm{p}}\gamma^{\mathrm{p}}}{\gamma_{\mathrm{w}}^{\mathrm{p}}+\gamma^{\mathrm{p}}}\right)$$

$$(1+\cos\theta_{\mathrm{EG}})\gamma_{\mathrm{EG}} = 4\left(\frac{\gamma_{\mathrm{EG}}^{\mathrm{d}}\gamma^{\mathrm{d}}}{\gamma_{\mathrm{EG}}^{\mathrm{d}}+\gamma^{\mathrm{d}}} + \frac{\gamma_{\mathrm{EG}}^{\mathrm{p}}\gamma^{\mathrm{p}}}{\gamma_{\mathrm{EG}}^{\mathrm{p}}+\gamma^{\mathrm{p}}}\right)$$

Surface tension components of water: $\gamma_W^P = 50.7 mNm^{-1}$, $\gamma_W^d = 22.1 mNm^{-1}$ $\gamma_W = 72.8 mNm^{-1}$, Ethylene glycol (EG): $\gamma_{EG}^P = 17.6 mNm^{-1}$, $\gamma_{EG}^d = 30.1 mNm^{-1}$, $\gamma_{EG} = 47.7 mNm^{-1}$ were based on the ref. 23. Then the polar component γ^p and the dispersive component γ^d of the surface tension of each polymer could be calculated.

Table 1. Contact Angles and Surface Tension Components of PU and PMMA Films

Polymer	Θ_w[a] (°)	Θ_{EG}[b] (°)	γ^p (mN m^{-1})	γ^d (mN m^{-1})
BD/1.7	78.6	40.7	12.6	24.9
BD/1.0	91.8	51.0	5.0	32.2
BisA/1.0	93.5	53.2	4.2	32.6
PMMA-BPO	85.3	44.1	8.2	29.5
PMMA-KPS	84.1	43.3	8.9	28.7

[a] Surface tension components of water: $\gamma_w^p = 50.7$ mN m^{-1}, $\gamma_w^d = 22.1$ mN m^{-1}, $\gamma_w = 72.8$ mN m^{-1}. [b] Surface tension components of ethylene glycol (EG): $\gamma_{EG}^p = 17.6$ mN m^{-1}, $\gamma_{EG}^d = 30.1$ mN m^{-1}, $\gamma_{EG} = 47.7$ mN m^{-1}.

Interfacial Tension Measurements (γ_{1w}, γ_{2w}, γ_{mw}, γ_{12}, and γ_{pw})

The interfacial tension measurements were done by the pendent drop method through Sinterface Tensiometer, PAT-2 with CCD camera. Interfacial tensions between monomer phase and water/SDS/KPS (if needed) (γ_{mw}), PU and water/SDS (γ_{1w}), PMMA and water/SDS (γ_{2w}) were measured at 70℃. For the measurement of γ_{mw}, the monomer phase included PU prepolymer, MMA, IPDI, BD or BisA, and TMP. A drop of monomer phase from a syringe was immersed into the water phase and γ_{mw} was calculated instantaneously by computer based on the shape of drop. Twelve weight ratios of monomer

phases were tested. Similarly, for the measurement of γ_{1w}, PU polymer was dissolved previously into IPDI and PPG monomers. And then the drop of PU/IPDI/PPG was immersed into water/SDS/KPS (if needed) phase. By increasing the concentration of PU polymer, a constant value of c was obtained and was regarded as c1w. In this work, there were four values of γ_{1w} (BD/BPO/1.7, BD/BPO1.0, BD/KPS/1.0, and BisA/KPS/1.0). For the measurement of γ_{2w}, PMMA polymer was dissolved into MMA monomer. The drop of PMMA/MMA was immersed into water/SDS/KPS (if needed) phase. By increasing the concentration of PMMA polymer, a constant value of γ was obtained and was regarded as γ_{2w}. In this work, there were two kinds of γ_{2w}, which were two types of PMMA polymers (PMMA-BPO, PMMAKPS).

The interfacial tension between PU and PMMA (γ_{12}) was calculated based on the results in Table 1 and the Harmonic-mean equation,23

$$\gamma_{12} = \gamma_1 + \gamma_2 - 4\left(\frac{\gamma_1^d \gamma_2^d}{\gamma_1^d + \gamma_2^d} + \frac{\gamma_1^p \gamma_2^p}{\gamma_1^p + \gamma_2^p}\right)$$

γ_1: Surface tension of PU polymer; γ_2: Surface tension of PMMA polymer.

γ_1^d and γ_1^p were the dispersive and polar components of surface tension of PU polymer, respectively.

γ_2^d and γ_2^p were the dispersive and polar components of surface tension of PMMA polymer,respectively.

And γ_{pw} in eq 9 was estimated according to the mixing rule (1-x) γ_{1w} + (x) γ_{2w}; x = PMMA/(PMMA+PU) weight ratio. Table 2 summarized the data of interfacial tensions of different systems.

Table 2. Interfacial tensions of monomer/water, PU/water, PMMA/water, and PU/PMMA

Polymer	PU/PMMA weight ratios[a]	γ_{mw} (10^{-3} N m^{-1})	γ_{1w}	γ_{2w}	γ_{12}[b]	γ_{pw}[c]
BD/1.7<->PMMA-BPO	20/80	4.6	2.9	4.9	1.3	4.50
	30/70	3.9				4.30
	40/60	3.4				4.10
BD/1.0<->PMMA-BPO	20/80	4.7	3.1	4.9	0.9	4.54
	30/70	4.0				4.36
	40/60	3.6				4.18
BD/1.0<->PMMA-KPS	20/80	3.4	2.9	3.5	1.3	4.42
	30/70	2.0				4.23
	40/60	1.4				4.04
BisA/1.0<->PMMA-KPS	20/80	3.3	2.9	3.5	1.9	3.38
	30/70	2.4				3.32
	40/60	1.8				3.26

[a] PU indicates the PU prepolymer, IPDI, TMP, and chain extenders.
[b] Based on Harmonic-mean equation.
[c] Based on $(1-x)\gamma_{1w} + (x)\gamma_{2w}$; x = PMMA/(PMMA+PU) weight ratio.

TEM Cross-Section Morphology

The morphology of particles of hybrid latex was characterized by TEM (JOEL JEM-1230 with Gatan DualVision CCD Camera). To observe the phase distribution in particles, the ultrathin cross section of the hybrid sample was stained by phosphotungstic acid (PTA) for 5 min. PTA can stain the PU phase but not the PMMA phase, so under the observation of TEM, the PU phase is dark, whereas the PMMA phase is bright.

RESULTS AND DISCUSSION

Contact Angles and Surface Tension Components of Polymer Films

Contact angles of five polymer films were shown in Table 1. For PU films, PU prepared with NCO/OH=1.7 had the lowest value of contact angle, which meant the highest hydrophilic property. Due to the hydrophilic property of BD chain extender, PU with BD chain extender showed the lower contact angle than PU with Bisphenol A chain extender. Furthermore, by comparing contact angles of PMMA films, PMMA synthesized with KPS initiator was more hydrophilic than PMMA with BPO initiator because of the ion charge of KPS.

Interfacial Tensions of Monomer/Water, PU/Water, PMMA/Water, and PU/PMMA

The interfacial tensions of monomers/water (γ_{mw}) were shown in Table 2. It was apparently affected by different weight ratios of PU/PMMA. In the existence of NCO-terminated PU prepolymer, monomer phase would turn into more hydrophilic and γ_{mw}

decreased. Hence, with increasing hydrophilic PU content, γ_{mw} decreased.

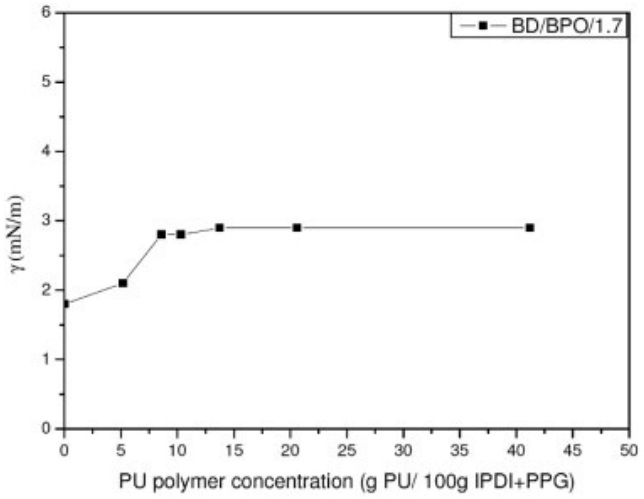

Figure 2. Interfacial tensions between PU+IPDI+PPG and water with different PU polymer concentrations for BD/BPO/1.7 system.

Besides, if excess IPDI was added (BD/1.7), it also resulted in a higher hydrophilic monomer phase and thus a lower γ_{mw} was obtained. To measure the interfacial tension of PU/water (γ_{1w}), PU polymer phase with different concentrations was dissolved previously into its monomers. As increasing PU polymer (BD/1.7) concentration, Figure 2 indicated the value of γ would increase in the beginning. It was because that PU polymer, which was hydrophobic than monomers, reduced the hydrophilic ability of monomer phase. As more PU polymer was added, γ approached a constant value at 2.9 mN m^{-1} and the value was regarded as the interfacial tension of PU(BD/1.7)/water (γ_{1w}). The same phenomenon was observed in the other PU polymer systems. Figure 3 revealed that the interfacial tension between PU polymer (BD/1.0) and water was 3.1 mN m^{-1}, which was higher than the value of PU polymer (BD/1.7). It could be seen that the higher amount of NCO groups indeed led to a higher hydrophilic monomer phase. Figures 4 and 5 showed the interfacial tension between PU polymer (BD/1.0) and water phase was 2.9 mN m^{-1}, as using BisA as the chain extender (BisA/1.0), γ was 2.9 mN m^{-1}.

Different initiators for MMA polymerization also influenced the interfacial tension. By using BPO as the initiator, as shown in Figure 6, the interfacial tension (c2w) between PMMA/MMA and water was 4.9 mN m^{-1}. However, when KPS was used as the initiator, Figure 7 showed that γ_{2w} reduced to 3.5 mN m^{-1}. PMMA prepared from KPS initiator had much lower value of γ_{2w} than PMMA synthesized by BPO initiator. It was ascribed to the ion charge of KPS that reducing the interfacial tension.

According to the Harmonic-mean equation, the interfacial tension (γ_{12}) of PU and PMMA was calculated by their contact angles. It could be seen that γ_{12} was much lower than the other interfacial tensions.

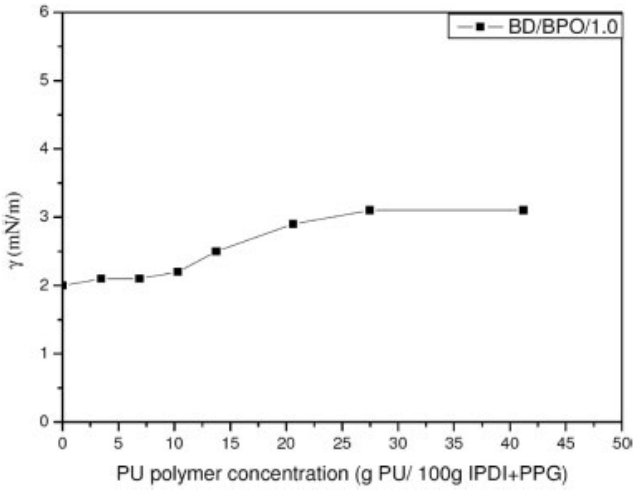

Figure 3. Interfacial tensions between PU+IPDI +PPG and water with different PU polymer concentrations for BD/BPO/1.0 system.

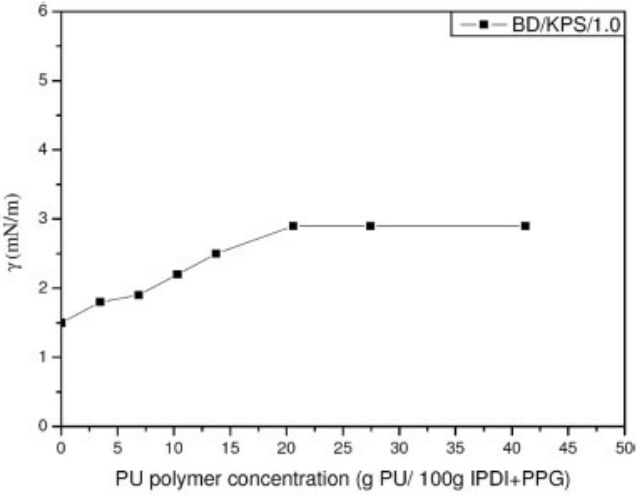

Figure 4. Interfacial tensions between PU+IPDI +PPG and water with different PU polymer concentrations for BD/KPS/1.0 system.

Consideration of Four PU/PMMA Systems

Based on interfacial tensions, the free energy changes of five final states with different PU/PMMA weight ratios could be calculated. The preferred morphology of PU/PMMA hybrid particle had a

minimum ΔG_{phase} value. As shown in Figure 8, BD/BPO system with NCO/OH= 1.7 had the order of free energy change A > C > E > B > D. The minimum ΔGphase was the state D, which had the three-layer structure. Since the state B only had a slightly higher value than the state D, it indicated that PU-rich phase as the shell and PMMA-rich as the core, was preferred than the other states.

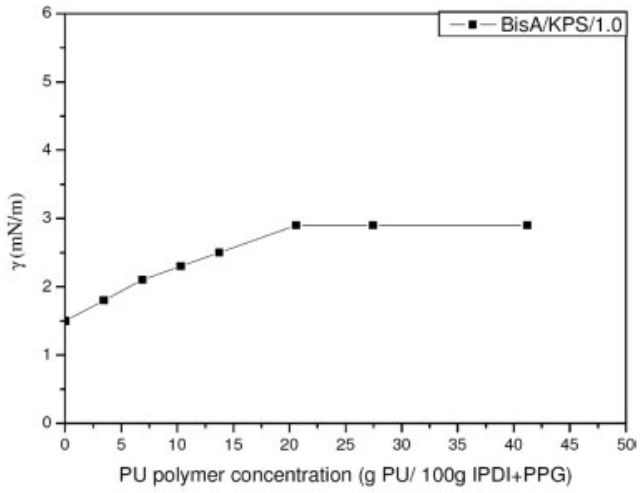

Figure 5. Interfacial tensions between PU+IPDI+PPG and water with different PU polymer concentrations for BisA/KPS/1.0 system.

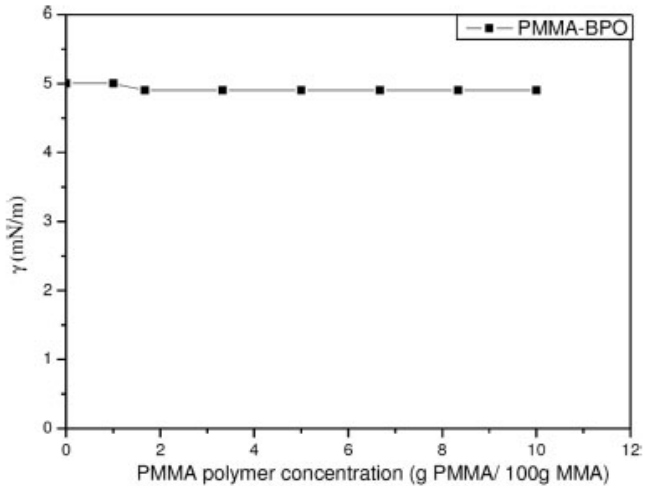

Figure 6. Interfacial tensions between PMMA-BPO/MMA and water with different PMMA polymer concentrations for PMMA-BPO system.

For BD/BPO systems with NCO/OH ratio=1.0, the free energy changes were shown in Figure 9; the order of free energy change, A–C > E > B > D, was similar to the result shown in Figure 8. The preferred morphology was still PU-rich phase as the shell and PMMA-rich as the core

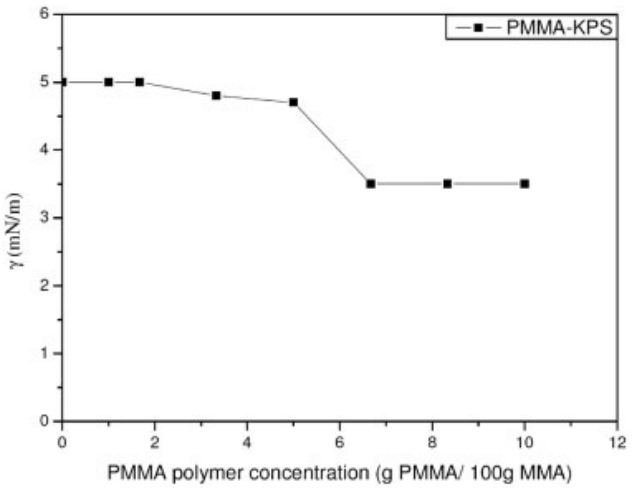

Figure 7. Interfacial tensions between PMMA-KPS/MMA and water with different PMMA polymer concentrations for PMMA-KPS system.

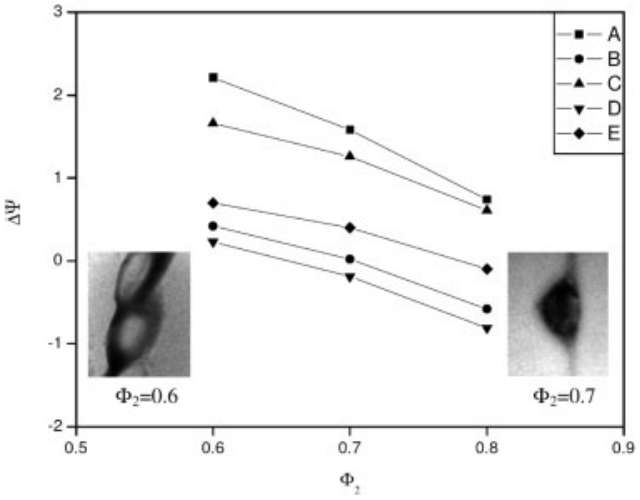

Figure 8. The predicted free energy changes of five final states for BD/BPO systems with NCO/OH= 1.7 and different volume fractions of PMMA. For case D, $\gamma_{23}=\gamma_{13}=\gamma_{12}/2$, R_2=10, R_0=Z-average diameter, $\Phi_{31}=\Phi_{32}$= 0.5 for consideration.

As shown in Figure 10, the order of free energy change was A > C > E > B > D. Using water-soluble KPS initiator, it led to less difference of free energy change among the five states comparing to the system with BPO initiator. Due to using KPS initiator, PMMA chain end would have more hydrophilic ions. Then the compatibility between PU and PMMA increased. From the calculation, the preferred structure was still PU-rich as the shell and PMMA-rich as the core.

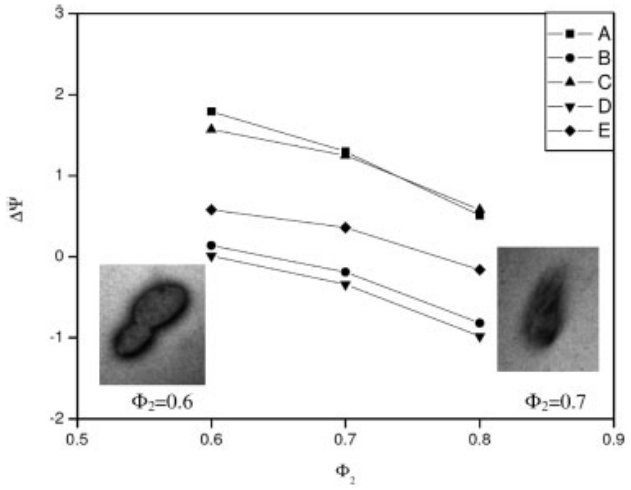

Figure 9. The predicted free energy changes of five final states for BD/BPO systems with NCO/OH=1.0 and different volume fractions of PMMA. For case D, $\gamma_{23} = \gamma_{13} = \gamma_{12}/2$, $R_2 = 10$, R_0 = Z-average diameter, $\Phi_{31} = \Phi_{32} = 0.5$ for consideration.

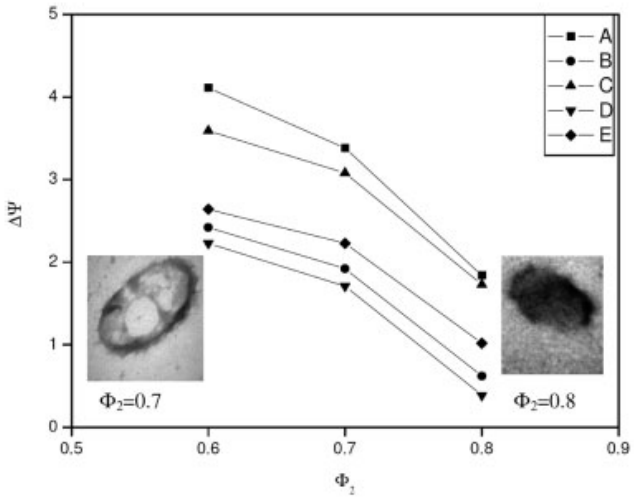

Figure 10. The predicted free energy changes of five final states for BD/KPS systems with NCO/OH= 1.0 and different volume fractions of PMMA. γ_{2W}=4.8 based on low conversion of MMA. For case D, $\gamma_{23} = \gamma_{13} = \gamma_{12}/2$, R_2=10, R_0= Z-average diameter, $\Phi_{31} = \Phi_{32} = 0.5$ for consideration.

In Figure 11, when incorporating bisphenol A as the chain extender, the difference of free energy changes among five states became smaller. It meant that using hydrophobic chain extender for PU would cause a better mixing of PU and PMMA phases. Hence, unlike previous systems, the state E showed the lowest free energy change, where the homogeneous structure was preferred. By comparing the interfacial tensions of γ_{1w} and γ_{2w}, PMMA/water had a higher interfacial tension than PU/water with BD chain extender. According to earlier papers,9,10 polymer/water with higher interfacial tension was formed preferentially at the core of hybrid particle. Hence, the PU with BD chain extender formed core-shell particles. While in the case of using BisA as chain extender of PU, the difference of γ_{1w} and γ_{2w} became quite small, thus the homogeneous morphology of hybrid particles was possibly formed.

According to above analyses, the influences of different NCO/OH ratios and initiators of MMA on the morphology of PU/PMMA hybrid particle were not obvious. Systems of BD/BPO/1.7, BD/BPO/1.0, and BD/KPS/1.0 showed PU-rich phase as the core and PMMA-rich as the shell. However, more hydrophobic chain extender in PU phase would affect largely the morphology of hybrid particles (BisA/KPS/1.0), and showed a homogeneous structure in hybrid particles.

Comparison of TEM Observation and the Predicted Morphology from Thermodynamic Consideration

BD/BPO/1.7 System

According to TEM cross section observation, the particle of PU/PMMA= 30/70 had a core-shell structure and it was more obvious for PU/PMMA=40/60. From thermodynamic consideration, as shown in Figure 8, the preferred final state was also a core-shell structure. The initial monomer droplet before polymerization was considered as a homogeneous phase. When a larger amount of MMA was used, the rate of polymerization of MMA became faster. Although the thermodynamically preferred state was core-shell, the core-shell structure was not very obviously observed in PU/PMMA=30/70 because of the rapid polymerization of MMA and the morphology of hybrid particles was quickly frozen during polymerization. It meant that the kinetic effect limited the approaching of thermodynamic equilibrium. When a less amount of MMA was used, the rate of polymerization of MMA turned into slower. Hence, the particle had a more obvious core-shell structure due to the slower rate of polymerization as seen in PU/PMMA=40/60.

BD/BPO/1.0 System

From TEM observation, PU/PMMA = 30/70 had a core-shell structure and it was more obvious for PU/PMMA=40/60. The

preferred morphology from the calculation was still core-shell. As explained above, PU/PMMA= 30/70 system had the faster rate of polymerization and the kinetic effect led to a less core–shell morphology. However, PU/PMMA=40/60 had the slower rate of polymerization and resulted in a more obvious core-shell structure as predicted from thermodynamic consideration.

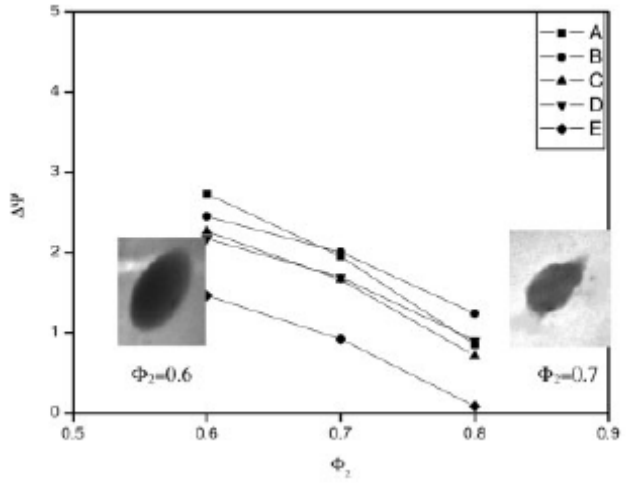

Figure 11. The predicted free energy changes of five final states for BisA/KPS systems with NCO/OH= 1.0 and different volume fractions of PMMA. For case D,$\gamma_{23}=\gamma_{13}=\gamma_{12}/2$, R_2=10, R_0= Z-average diameter, $\Phi_{31}=\Phi_{32}$= 0.5 for consideration.

BD/KPS/1.0 System

The morphologies of TEM observation showed that PU/PMMA 20/80 was less of core-shell whereas PU/PMMA=30/70 was clear in coreshell. From thermodynamic consideration, the preferred state was a core-shell structure. The reason for different morphologies of TEM observation was the same as discussed before. PU/PMMA= 20/80 had a faster rate of polymerization, hence, the kinetic effect caused less coreshell structure. On the contrary, PU/PMMA 30/70 showed a more obvious core-shell structure due to its slower polymerization.

BisA/KPS/1.0 System

From TEM observation, both PU/PMMA= 30/70 and 40/60 of BisA/KPS/1.0 showed homogeneous structure. And the preferred morphology from the thermodynamic calculation was also homogeneous. Unlike the previous three systems, BisA/KPS/1.0 preferred the homogeneous structure and the kinetic effect was not important, because the initial state was homogeneous.

CONCLUSIONS

Based on the interfacial tensions, the free energy changes of five final states of hybrid particles with different PU/PMMA weight ratios can be calculated by thermodynamic consideration. The preferred morphology of PU/PMMA hybrid particle had the minimum free energy change. BD/BPO systems with different NCO/OH ratio showed that the minimum free energy change was state D, which was a three layer structure, that is, PU phase as the shell, PMMA phase as the core, and an intermediate layer of PU/PMMA. Using KPS initiator instead, PMMA chain end would have more hydrophilic ions. The preferred structure was still PU-rich as the shell and PMMA-rich as the core. When incorporating bisphenol A as the chain extender of PU, the free energy changes of five states became closer. It meant that using hydrophobic chain extender would cause a better mixing of PU and PMMA phases. Hence, unlike other systems, the state E showed the lowest free energy change, where the homogeneous structure of hybrid particles was preferred for system BisA/KPS/1.0.

REFERENCE

1 Frisch, K. C.; Klempener, D.; Migdal, S. Polym Eng Sci 1974, 15, 76–78.

2 Mohammed, S.; Daniels, E. S.; Sperling, L. H.; Klein, A.; El-Aasser, M. S. J Appl Polym Sci 1997, 66, 1869–1884.

3 Mishra, V.; Prez Du, F. E.; Gosen, E.; Goethals, E. J.; Sperling, L. H. J Appl Polym Sci 1995, 58, 331–346.

4. Wang, C.; Chu, F.; Graillat, C.; Guyot, A.; Guyot, C. Polym Adv Technol 2005, 16, 139–145.

5. Okubo, M.; Katsuta, Y.; Matsumoto, T. J Polym Sci Polym Chem Ed 1980, 18, 481–486.

6. Li, M.;Daniels, E.S.; Dimonie, V.;Sudol, E.D.; El-Aasser, M. S. Macromolecules 2005, 38, 4183–4192.

7. Wang, C.; Chu, F.; Graillat, C.; Guyot, A.; Gauthier, C.; Chapel, J. P. Polymer 2005, 46, 1113–1124.

8. Gooch, J. W.; Dong, H.; Schork, F. J. J Appl Polym Sci 2000, 76, 105–114.

9. Chen, Y. C.; Dimonie, V.; El-Aasser, M. S. J Appl Polym Sci 1991, 42, 1049–1063.

10. Chen, Y. C.; Dimonie, V.; El-Aasser, M. S. J Appl Polym Sci 1992, 45, 487–499.

11. Okubo, M.; Yamada, A.; Matsumoto, T. J Polym Sci Polym Chem Ed 1980, 16, 3219–3228.
12. Okubo, M.; Katsuta, Y.; Matsumoto, T. J Polym Sci Polym Chem Ed 1982, 20, 45–51.
13. Torza, S.; Mason, S. J Colloid Interface Sci 1970, 33, 67–76.
14. Dimonie, V. L.; El-Aasser, M. S.; Vanderhoff, J. W. Polym Mater Sci Eng 1988, 58, 821–832.
15. Chen, Y. C.; Dimonie, V.; El-Aasser, M. S. Macromolecules 1991, 24, 3779–3787.
16. Sundberg, D. D.; Casassa, A. P.; Pantazopoulos, A. P.; Muscato, M. R. J Appl Polym Sci 1990, 41, 1425–1442.
17. Kwok, D. Y.; Neumann, A. W. Can J Chem Eng 1996, 74, 551–553.
18. Lando, J. L.; Oakley, H. T. J Colloid Interface Sci 1967, 25, 526–530.
19. Potschke, P.; Pionteck, J.; Stutz, H. Polymer 2002, 43, 6965–6972.
20. Venugopal, G.; Krause, S. Macromolecules 1992, 25, 4626–4634.
21. Guschl, P. C.; Otaigbe, J. U. J Colloid Interface Sci 2003, 266, 82–92.
22. Rusanov, A. I.; Prokhorov, V. A. Interfacial Tensiometry; Elsevier: Amsterdam, 1996.
23. Wu, S. Polymer Interface and Adhesion; Marcel Dekker Inc.: New York, 1982.

PARTⅤ：Synthesis of ZnO/Polystyrene Composites Particles by Pickering Emulsion Polymerization

ABSTRACT

ZnO/polystyrene composite particles were synthesized by Pickering emulsion polymerization. ZnO nanoparticles were first prepared by reaction of zinc acetate and sodium hydroxide in ethanol medium. Then different amount of styrene monomer was emulsified in water in the presence of ZnO nanoparticles either by mechanical stirring or by sonication, followed by polymerization of styrene. Two kinds of initiators were used to start the polymerization, Azobisisobutyronitrile (AIBN) and potassium persulfate (KPS). The X-ray diffraction pattern verified the crystal structure of ZnO and FT-IR spectra evidenced the existence of ZnO and polystyrene (PS) in ZnO/polystyrene composite particles. Different morphologies were observed for the composite particles when using different initiators. From TEM photographs, AIBN-initiated system produced mainly core-shell composite particles with PS as core and ZnO as shell, while KPS-initiated system showed both composite particles and pure PS particles. Two schemes of reaction mechanism were proposed to explain the morphologies accordingly. Two systems of composite particles showed good pH adjusting ability.

Key words: ZnO, polystyrene, composite particles, Pickering emulsion polymerization.

1. Introduction

In recent years, many efforts have been focused on the inorganic/organic composite materials with various compositions. By combining organic and inorganic materials, the resulting composites can possess advantages of both organic and inorganic components, thus creating extensive usages in many areas. Among the many inorganic materials, zinc oxide, ZnO, is a direct band-gap (Eg = 3.37 eV) semiconductor with a large exciton binding energy (60 meV)[1]. Therefore ZnO is useful in many application areas such as solar cell[2], gas sensor[3,4], varistors[5], acoustic, and luminescent devices[6-8]. Generally, ZnO can be synthesized by sol-gel method[9,10], homogeneous precipitation[11], chemical vapor deposition[12], thermal decompostition[13,14], hydrothermal synthesis[15], and reaction of zinc salt with base[16]. Different synthesis routes result in different ZnO morphology, including particle, rod, tube, and flower-like. Moreover, ZnO is also an amphoteric substance and has the ability to sense[17] and adjust pH value, making it useful in biomaterial and textile.

Traditional emulsion polymerization was proceeded by adding surfactant to stabilize hydrophobic monomer in aqueous medium. If surfactants are replaced by inorganic nano-sized particles it is called Pickering emulsion polymerization, which was proposed by Pickering in 1907[18]. Theoretical and experimental researches of Pickering emulsion polymerization were developed by He[19-21] and Blinks[22,23]. When the size of inorganic particle is reduced to nanoscale, they are able to adsorb on the surfaces of monomer droplets to form a stable dispersion. After polymerization inorganic/polymer composite particles can be obtained. In this paper, ZnO/polystyrene composite particles were prepared by Pickering emulsion polymerization. ZnO nanoparticles were first synthesized from reaction of zinc acetate and sodium hydroxide in ethanol. Then polymerization of styrene with different initiators was conducted in the presence of ZnO nanoparticles. The crystal structure was studied with X-ray diffraction and the functional groups of both inorganic and organic components were characterized with Fourier transform infrared spectroscope. The morphology of ZnO/polystyrene composite particles was studied with transmission electron microscopy. Finally the pH adjusting ability of ZnO/polystyrene composite particles was investigated.

2. Experiments

2.1 Materials

Zinc acetate and sodium hydroxide (NaOH) purchased from Acros were used as precursor and base in the synthesis of ZnO nanoparticles. Styrene monomer (St) was also purchased from Acros and used as received. Azobisisobutyronitrile (AIBN) and potassium persulfate (KPS) were used as initiators of polymerization of styrene. Ethanol and DI-water were used as solvents of synthesis of ZnO nanoparticles and Pickering emulsion polymerization, respectively.

2.2 Preparation of ZnO nanoparticles

ZnO nanoparticles can be prepared by the reaction of zinc acetate

and a base in the alcohol medium. In this study, 1.314g zinc acetate and 0.48g NaOH were dissolved in 330ml ethanol and refluxed at 60^{o}C for 1h. The acetate group reacted with base, converting zinc acetate into zinc oxide. After reaction, the zinc oxide ethanol dispersion was mixed with DI-water for purification. ZnO particles were then separated from the dispersion supernatant by centrifugation at 7000 rpm for 5 minutes repeatedly. Finally the ZnO particles were redispersed in DI-water to obtain ZnO water dispersion. TEM result indicated that the size of ZnO particles were about 10-30nm, as shown in Fig. 1.

2.3 Pickering emulsion polymerization of ZnO/polystyrene composite particles

For AIBN-system, styrene monomer and AIBN were first mixed with 10ml DI-water and then added to 50ml of ZnO water dispersion prepared as described in section 2.2. The mixture was then emulsified either by mechanical stirring (300rpm) or sonication with a Dr. Hielscher UP50H at 100% amplitude under 0^{o}C for 10 minutes. After emulsification, the minieulsion was heated to 75^{o}C to start the polymerization of styrene under stirring (300rpm) and a nitrogen atmosphere. After 6hr of polymerization, the ZnO/polystyrene composite latex was diluted with methanol and separated from the dispersion supernatant by centrifugation at 13000 rpm for 15 minutes repeatedly. As for KPS-system, KPS was added after the miniemulsion of ZnO and styrene was heated to 75^{o}C. The ZnO/polystyrene composite particles were dried to powder in an oven for further characterization. The compositions of recipes to prepare different ZnO/polystyrene composite particles were listed in Table 1.

2.4 Characterization

X-ray diffraction (XRD) patterns were taken to analyze the crystal structures of ZnO, using a MAC Science/MXP X'pert diffractometer with CuKα radiation at 40 KV and 30mA. ZnO/polystyrene composite particles were pressed into KBr pellet and the Fourier transform infrared spectrum (FT-IR) was obtained with BIO-RAD FTS40 in the 400-4000 cm^{-1} range with 16 scans. The morphology of ZnO/polystyrene composite particles was observed with a Hitachi H-7100 transmission electron microscope (TEM).

2.5 pH adjusting ability

The pH adjusting ability of ZnO/polystyrene composite particles was investigated by dispersing ZnO/polystyrene composite particles into water solution with different pH value to form 1000 ppm ZnO/polystyrene water dispersion. For example, 0.01g ps1ZnO(A) was added to 10ml of water solutions with pH=3, 5, 7, and 9 for 10 minutes. Then the pH values before and after ZnO/polystyrene dispersion were recorded and compared.

3. Results and discussions

3.1 XRD analysis of ZnO/polystyrene composite particles

The XRD patterns of ZnO, ZnO/polystyrene composites and polystyrene were shown in Fig 2. Pure ZnO particles possess main peaks at 2θ=32^{o}, 34.4^{o}, 36.6^{o}, corresponding to (100), (002), and (101) planes, respectively[24]. In this study, ZnO was synthesized from zinc acetate and base. The by-product sodium acetate could be dissolved in water and removed by centrifugation. Therefore sodium acetate was not observed on XRD pattern. The XRD patterns of ZnO/polystyrene composite particles of different compositions were almost the same as that of ZnO, indicating that the crystal structure of ZnO was not altered by the presence of polystyrene. In a Pickering emulsion polymerization, ZnO particles played a role as surfactant, which adsorbed on the surfaces of polystyrene/St particles to form a stable latex. As a result the XRD pattern of ZnO/polystyrene composite particles exhibited the same characteristics of ZnO.

3.2 FT-IR analysis of ZnO/polystyrene composite particles

Fig. 3 showed the FT-IR spectra of ZnO, polystyrene, and PS3ZnO composite particles. ZnO/polystyrene composite and polystyrene presented the same spectra in the wavenumber range of 700-3100 cm^{-1} while the weak peak located at 500-700cm^{-1} is attributed to the stretching of Zn-O bond. Since the characteristic peaks of polystyrene and ZnO are both presented on PS3ZnO spectrum, it is clear that ZnO/polystyrene composite was successfully synthesized in this work.

3.3 Morphology study of ZnO/polystyrene composite particles

The ZnO/polystyrene composite particles in this study can be classified as polymerization initiated by AIBN and by KPS.

During the emulsification process of styrene monomer and ZnO dispersion, styrene is a hydrophobic monomer and no surfactant was added, but phase separation was not observed. It indicated that styrene monomer is well-protected by ZnO nanoparticles to form a stable suspension in water. ZnO nanoparticles acted as surfactants.

3.3.1 AIBN system

The hydrophobic initiator AIBN was existing in the styrene droplets to initiate polymerization. The nucleation mechanism of polymer particles in such case is mainly droplet nucleation. The sizes of monomer droplets and polymer latex particles were almost identical. Fig. 4 to Fig. 6 showed the morphologies of PS1ZnO(A), PS2ZnO(A), and PS3ZnO(A) respectively. It was seen that the surfaces of polystyrene particles were covered with ZnO nanoparticles, showing a core-shell structure. As the content of styrene increased from 0.1g to 0.3g in the reaction recipes in Table1, the size of ZnO/polystyrene composite particles increased from about 50nm to 200nm. When the content of monomer was higher, the relative concentration of ZnO to styrene decreased, and it tended to form larger droplets during emulsification, resulting in larger size of ZnO/polystyrene composite particles. The emulsification methods also affected the particle size. When the content of styrene monomer was 0.1g or 0.2g, the degree of emulsification by mechanical stirring and that by sonication were comparative. Therefore comparing Fig. 4 with Fig. 7 or Fig. 5 with Fig. 8, particle sizes of PS1ZnO(A) and PS1ZnOs(A) or PS2ZnO(A) and PS2ZnOs(A) were similar. As the content of styrene monomer increased to 0.3g, emulsification by sonication resulted in particle size of 120nm, shown in Fig. 9, nearly half of that of PS3ZnO(A). Therefore, the size of ZnO/polystyrene composite particles can be controlled by monomer content (or relative concentration of ZnO to styrene) and emulsification methods.

3.3.2 KPS system

When KPS was used as the initiator, the morphology of composite particles was very different. KPS is a hydrophilic initiator. The nucleation of polymer particles occurred not only in monomer droplets but also in water phase. When the content of styrene was low, as for PS1ZnO(K) shown in Fig. 10, large portion of pure PS particles was observed in addition to composite particles with ZnO nanoparticles on the surface, which indicated that major part of the nucleation of polymer particles occurred in water. As the content of styrene increased to 0.2g and 0.3g for PS2ZnO(K) and PS3ZnO(K), respectively, the number of styrene droplets increased. Therefore more radicals from KPS would be captured by styrene droplets and the proportion of nucleation in droplets would be raised. On the other hand, the ratio of ZnO to styrene decreased as a consequence of styrene increasing. The ZnO/polystyrene composite latex became less stable for the lack of ZnO nanoparticles as surfactants. As a result, coagulation occurred from time to time as seen in Fig. 11 and Fig. 12 for PS2ZnO(K) and PS3ZnO(K), respectively. Three kinds of particles were observed: PS with ZnO nanoparticles on the surfaces due to nucleation in droplets, pure PS particles due to nucleation in water, and ZnO-embedded PS particles due to coagulation of particles.

Looking into the morphologies of latex particles emulsified by sonication instead of mechanical stirring, since the number of styrene droplets increased after sonication, the probability of droplet nucleation would be enhanced, as shown in Fig. 13 for PS1ZnOs(K). However, when styrene monomer was increased to 0.2g or 0.3g for PS2ZnOs(K) and PS3ZnOs(K), respectively, the relatively insufficient ZnO nanoparticles resulted in less stable droplets, thus both nucleation in water and coagulation of particles increased. It can be seen from Fig. 14 for PS2ZnOs(K) and Fig. 15 for PS3ZnOs(K) that pure PS particles nucleated in water and coagulation thus formed large composite particles were together existing in the reaction systems.

From the discussion above, the mechanism of Pickering emulsion polymerization of ZnO and polystyrene can be summarized as scheme 1 and scheme 2. For AIBN system, styrene monomer was well-protected by ZnO nanoparticles and polymerization reaction occurred mainly in styrene droplets, since AIBN was a hydrophobic initiator. The resulting composite particles showed core-shell morphology. The difference in morphology of particles between mechanical stirring and sonication on emulsification was only apparent when the content of styrene was high. For KPS system, the proportion of polymer particle nucleation in droplets decreased but nucleation in water increased due to the hydrophilic property of KPS. Both pure PS particles and ZnO/PS composite

particles were observed. Besides, coagulation of particles resulted in ZnO-embedded morphology.

3.4 pH adjusting ability investigation

ZnO is an amphoteric substance that can react with either an acid or a base. In a acid medium, ZnO reacts with proton to form Zn^{2+} and H_2O, while in a base medium, ZnO reacts with hydroxide group to form $[Zn(OH)_4]^{2-}$. This property makes ZnO a good material for pH adjusting. In this study, the variation of pH value of 1000 ppm of ZnO/polystyrene water dispersion with different pH was compared. As shown in Fig. 16, both ZnO/polystyrene composite particles initiated by AIBN and KPS adjusted water solution from pH=3, 5, 7, or 9 to pH=7~8. That is, ZnO/polystyrene composite particles as-prepared could adjust acid and base solution to neutral. They are potential to be good pH adjusting materials. To increase the range of pH adjusting and their application are under study.

4. Conclusion

By Pickering emulsion polymerization, ZnO/polystyrene composite particles were successfully synthesized. ZnO nanoparticles acted as surfactant in the polymerization of styrene. The crystal structure of ZnO in ZnO/polystyrene composite particles was not altered. Using different initiators in the polymerization, it resulted in different morphologies of ZnO/polystyrene composite particle. Due to the difference of degree of hydrophilicity, AIBN initiated system resulted in ZnO-shell and PS-core composite particles while KPS initiated system resulted in pure PS particles and composite particles with ZnO on the surface or ZnO embedded inside. ZnO/polystyrene composite particles showed good pH adjusting ability and they are potential as a pH buffering material.

Reference

(1) Yi, G.-C.; Wang, C.; Park, W. I. *Semiconductor Science and Technology* **2005**, *20*, S22-S34.

(2) Beek, W. J. E.; Wienk, M. M.; Janssen, R. A. J. *Journal of Materials Chemistry* **2005**, *15*, 2985-2988.

(3) Sahay, P. P. *Journal of Materials Science* **2005**, *40*, 4383.

(4) Jiaqiang, X.; Yuping, C.; Daoyong, C.; Jianian, S. *Sensors and Actuators, B: Chemical* **2006**, *113*, 526-531.

(5) Kong, L.; Li, F.; Zhang, L.; Yao, X. *Journal of Materials Science Letters* **1998**, *17*, 769-771.

(6) Hao, X. T.; Zhu, F. R.; ONg, K. S.; Tan, L. W. *Semiconductor Science and Technology* **2006**, *21*, 48-54.

(7) Shih, W.-C.; Wu, M.-S. *Journal of Crystal Growth* **1994**, *137*, 319-325.

(8) Radovanovic, R. V.; Norberg, N. S.; McNally, K. E.; Gamelin, D. R. *Journal of the American Chemical Society* **2002**, *129*, 15192-15193.

(9) Khrenov, V.; Klapper, M.; Koch, M.; Mullen, K. *Macromolecular Chemistry and Physics* **2005***206*, 95-101.

(10) Toutorski, I. A.; Tkachenko, T. E.; Pokidko, B. V. *Journal of Sol-Gel Science and Technology* **2003**, *26*, 505-509.

(11) Taubert, A.; Palms, D.; Weiss, Ö.; Piccini, M.-T.; Batchelder, D. N. *Chemistry of Materials* **2002**, *14*, 2594-2601.

(12) Purica, M.; Budianu, E.; Rusu, E.; Danila, M.; Gavrila, R. *Thin Solid Films* **2002**, *403-404*, 485-488.

(13) Audebrand, N.; Auffrédic, J.-P.; Louër, D. *Chemistry of Materials* **1998**, *10*, 2450-2461.

(14) Yang, Y.; Chen, H.; Zhao, B.; Bao, X. *Journal of Crystal Growth* **2004**, *263*, 447-453.

(15) Lu, C.-H.; Yeh, C.-H. *Ceramics International* **2000**, *26*, 351-357.

(16) Trindade, T.; Jesus, J. D. P. d.; O'Brien, P. *Journal of Materials Chemistry* **1994**, *4*, 1615-1617.

(17) Al-Hilli, S. M.; Al-Mofarji, R. T.; Willandera, M. *Applied Physics Letters* **2006**, *89*, 173119.

(18) Pickering, S. U. *Journal of Chemical Society* **1907**, *91*, 2001-2021.

(19) He, Y. *Powder Technology* **2004**, *147*, 59-63.

(20) He, Y. *Applied Surface Science* **2005**, *249*, 1-6.

(21) He, Y.; Li, K. *Journal of Colloid and Interface Science* **2007**, *306*, 296-299.

(22) Binks, B. P.; Lumsdon, S. O. *Langmuir* **2000**, *16*, 8622-8631.

(23) Binks, B. P.; Clint, J. H. *Langmuir* **2002**, *18*, 1270-1273.

(24) He, Y.; Sang, W.; Wang, J. a.; Wu, R.; Min, J. *Journal of Nanoparticle Research* **2005**, *7*, 307-310.

Table 1 composition of recipes to prepare ZnO/polystyrene composite particles

sample	Styrene monomer	ZnO dispersion	Emulsification	Initiator [a]
PS1ZnO(A) PS2ZnO(A) PS3ZnO(A)	0.1g 0.2g 0.3g	50 ml	Mechanical stirring	AIBN
PS1ZnOs(A) PS2ZnOs(A) PS3ZnOs(A)	0.1g 0.2g 0.3g	50 ml	Sonification	AIBN
PS1ZnO(K) PS2ZnO(K) PS3ZnO(K)	0.1g 0.2g 0.3g	50 ml	Mechanical stirring	KPS
PS1ZnOs(K) PS2ZnOs(K) PS3ZnOs(K)	0.1g 0.2g 0.3g	50 ml	Sonification	KPS

[a] weight of initiator is 1% of weight of styrene monomer

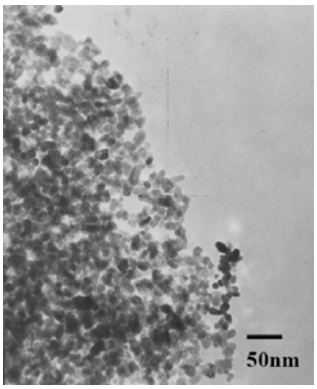

Fig.1 TEM of ZnO nanoparticles

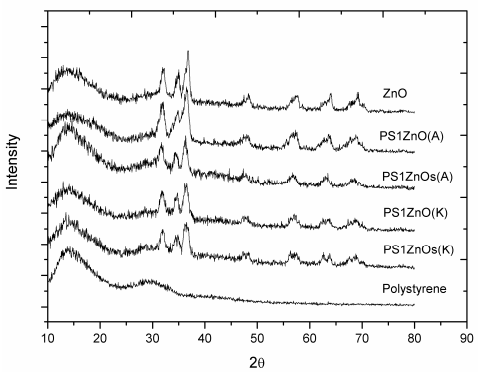

Fig. 2 XRD patterns of ZnO, ZnO/polystyrene composites and polystyrene

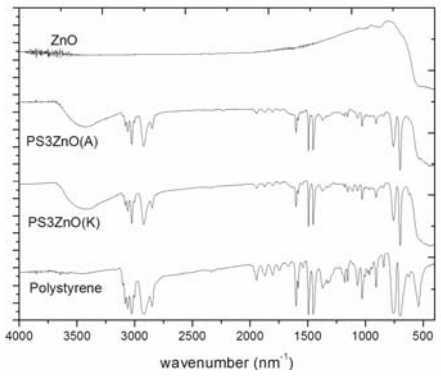

Fig. 3 FT-IR spectra of ZnO, polystyrene, and PS3ZnO composite particles

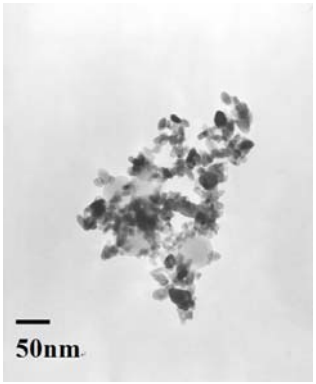

Fig. 4 TEM of PS1ZnO(A)

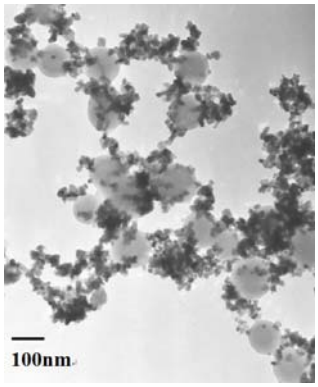

Fig. 5 TEM of PS2ZnO(A)

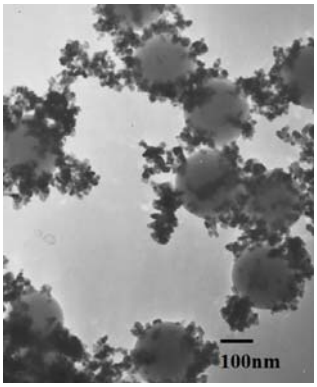

Fig. 6 TEM of PS3ZnO(A)

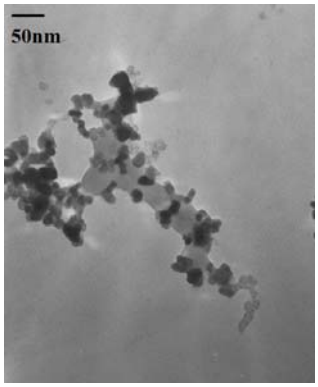

Fig. 7 TEM of PS1ZnOs(A)

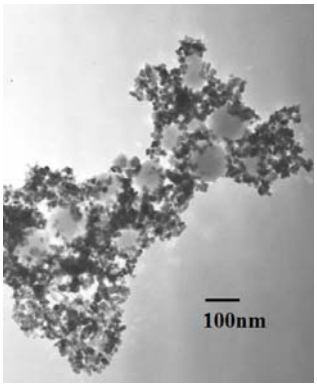

Fig. 8 TEM of PS2ZnOs(A)

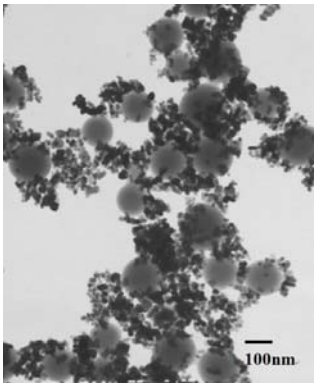

Fig 9 TEM of PS3ZnOs(A)

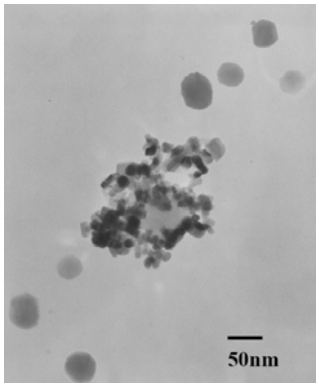

Fig. 10 TEM of PS1ZnO(K)

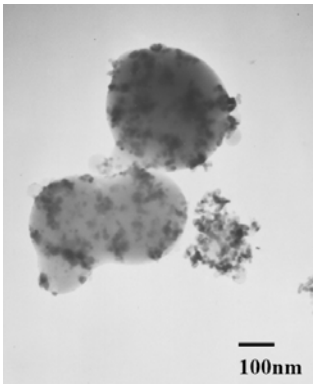

Fig. 11 TEM of PS2ZnO(K)

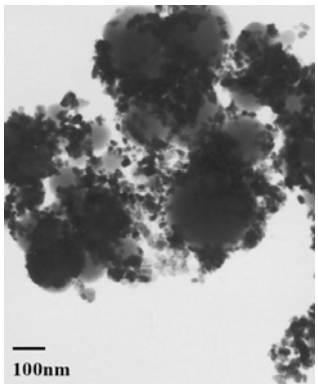

Fig. 12 TEM of PS3ZnO(K)

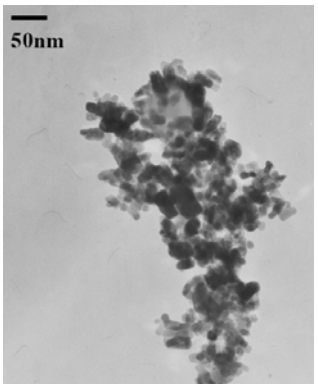

Fig. 13 TEM of PS1ZnOs(K)

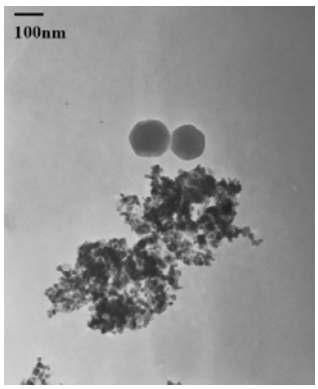

Fig. 14 TEM of PS2ZnOs(K)

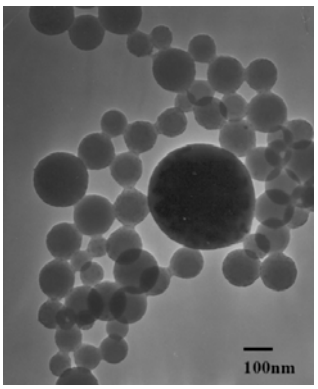

Fig. 15 TEM of PS3ZnOs(K)

59

Scheme 1 Mechanism of Pickering emulsion polymerization of ZnO and polystyrene initiated by AIBN

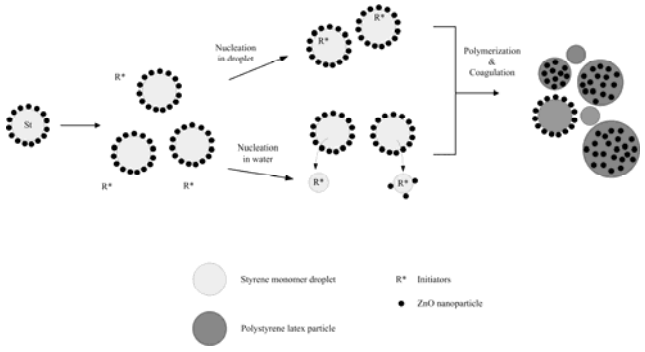

Scheme 2 Mechanism of Pickering emulsion polymerization of ZnO and polystyrene initiated by KPS

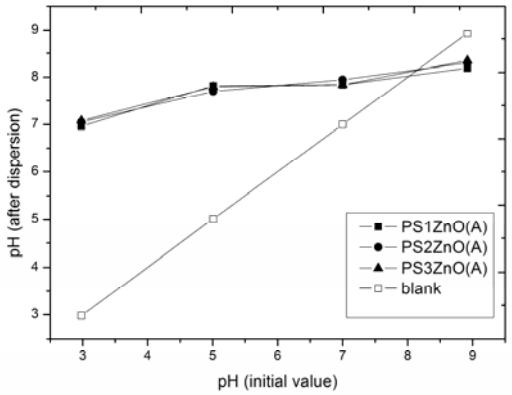

Fig. 16a. pH adjusting ability test of ZnO/Polystyrene composite particles initiated by AIBN (x axis: the initial pH value of solution ; y axis: the pH value after ZnO/Polystyrene composite particles dispersion; open squars: the blank test.)

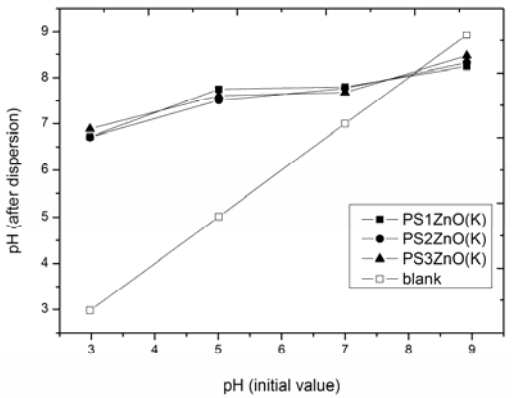

Fig. 16b. pH adjusting ability test of ZnO/Polystyrene composite particles initiated by KPS(x axis: the initial pH value of solution ; y axis: the pH value after ZnO/Polystyrene composite particles dispersion; open squares: the blank test.)

參加第232 屆美國化學學會會議心得報告

台大化工系邱文英

本人得到國科會補助，參加第232屆美國化學學會會議(The 232h ACS National Meeting)，此會議於2006 年9 月10 日~9 月14 日在美國舊金山舉行。這是一個很大型很有規模和歷史的會議，分成邀請演講、論文報告、海報及展覽，討論主題很廣，會場分散，本人主要參加了Colloid and surface chemistry，Polymeric materials及 Polymer chemistry三大項。

在Colloid and surface chemistry分項，共有21個主題，其中較有興趣的主題有

1. Multicompartment Micelles: Higher Order Self-Assembly of Block Copolymers
2. Organic Approaches to Nanotechnology
3. The Structure and Reactivity of Nano-particles in the Environment

在Polymeric materials分項，共有22個主題，其中較有興趣的主題有

1. General Papers/New Concepts in Polymeric Materials
2. Nanotechnology Applications in Coatings
3. Science and Technology of Next Generation Photovoltaics
4. Block Copolymers as Nanoscale Materials
5. Electroactive and Photoresponsive Metal-Containing Polymers
6. Advanced Membrances for Energy and Environmental Applications
7. Polymers for Biomedical Applications
8. Self-Assembly Approaches for Nanopatterning
9. Advanced in Protein Drugs and Gene Delivery: Delivery and Diagnostic Technologies
10. Fuel Cell Chemistry and Operation
11. Organic Thin Films for Photonic Application

在Polymer chemistry分項，共有19個主題，其中較有興趣的主題有

1. Polymers in Biosensors and Biochips
2. Multicompartment Micelles: Higher Order Self-Assembly of Block Copolymers
3. Nanoparticles and Microparticles: Synthesis and Applications
4. Biocatalysis in Polymer Science
5. Organic Thin Films for Photonic Applications
6. Silicones and Silicone-Modified Materials

演講及參與學者來自世界各國，包括美國、歐洲、日本、大陸及台灣等，從

這種大型會議，可以見識到在各領域的最近研究發展，對於自己的研究啟發一些新的想法。

本人在這次會議有三篇海報論文發表，

1. Preparation of resin black matrix (RBM) and their properties study
2. Synthesis of highly conductive self-doping poly(EDOT-co-TEBS) copolymer
3. Preparation of PU/PMMA hybrid latex by miniemulsion polymerization

其中第1 和2 篇被選擇在Joint PMSE/poly Poster session發表，第3 篇在Colloid surface chemistry Poster session 發表。三篇論文的摘要如下：

Preparation of resin black matrix (RBM) and their properties study

The object of this research was to investigate the effects of the composition on the UV curing and properties of the resin black matrix (RBM). Bisphenol A epoxy acrylate, Benzophenone tetracarboxylic dianhydride (BTDA), Isophorone diisocyanate (IPDI), and 2-Hydroxyethyl methacrylate (HEMA) were used to synthesize acrylic resin. VP-DP 9850 was used as dispersant of carbon black. Irgacure 242 was a proper photoinitiator. PGMEA was used as a solvent. Carbon black was surface treated with dispersant and stable dispersion could be obtained by ball milling. High optical density (about 4/μm) and 25μm line width of the resin black matrix could be prepared. The thermal decomposition temperature of the resin black matrix is higher than 350°C.

Synthesis of highly conductive self-doping poly(EDOT-co-TEBS) copolymer

The synthesis of poly(EDOT-*co*-TEBS) by oxidative polymerization in methanol was studied. The sodium sulfonate functional group on TEBS was introduced to PEDOT, leading to a conducting polymer with self-doping structure, therefore reducing the surface resistance. The experimental results indicated that the surface resistance was low when TEBS/EDOT molar ratio was between 2/15 to 3/15. Insufficient amount of TEBS caused poor doping effect while excess amount of TEBS would not completely dissolve in methanol for copolymerization. The content of initiator, $Fe(OTs)_3$, changed the polymerization rate, thus influenced the surface resistance of as prepared poly(EDOT-*co*-TEBS). Insufficient amount of $Fe(OTs)_3$ was difficult to initiate the reaction while excess amount of $Fe(OTs)_3$ overdoped the product. The concentration of Imidazole then affected the reaction mechanism and the structure of copolymers. The solid content of reaction mixture and film forming condition also affected properties of films. Surface resistance was lowered by four-fold when solid content increased from 10% to 40%. Transparent films could be obtained when higher spin-coating speed and longer spin time were applied.

Preparation of PU/PMMA hybrid latex by miniemulsion polymerization

PU/PMMA hybrid particles were synthesized by using the method of two-step miniemulsion polymerization. In the first step, PU prepolymer was synthesized by isophorone diisocyanates (IPDI) and poly (propylene glycol) (PPG) with methyl methacrylate (MMA) as a solvent. Then the oil phase, including the NCO-terminated prepolymer, MMA, hexadecane (HD), a chain extender, a cross-linking agent trimethylol propane (TMP), and a catalyst dibutyltin dilaurate (SnDBL) was dispersed in the water phase containing SDS. Then the mixtures turned into miniemulsion by ultrasonifying. Different chain extenders, such 1,4-butanediol (BD) and Bisphenol A (BisA), were used for PU prepolymer. Two kinds of initiators, BPO and KPS, were applied for the radical polymerization of MMA. The influences of chain extenders, initiators and PU/PMMA weight ratios on the morphology of PU/PMMA latex particles were investigated. Conversion of MMA was measured and discussed as well. Particle size and distribution were analyzed by dynamic lighting scattering (DLS). Thermal stability of the hybrid particle was characterized through thermal gravimetric analysis (TGA). The final cross-section morphology of hybrid latex was also characterized by transmission electron microscope (TEM).

在海報會場，大約有六、七百篇論文發表，本人也藉機會參觀別人的論文，並互相討論，受益良多，非常感謝國科會的補助和支持。